Evaluation of stratospheric intrusions and biomass burning plumes on the vertical distribution of tropospheric ozone over the Midwestern U.S.

J. L. Wilkins[1,2], B. de Foy[2], A. M. Thompson[3], D. A. Peterson[4], E. J. Hyer[4], C. Graves[2], J. Fishman[2], and G. A. Morris[5]

[1]Office of Research and Development, U.S. Environmental Protection Agency, Research Triangle Park, USA, [2]Department of Earth and Atmospheric Sciences, St. Louis, MO, USA, [3]NASA/Goddard Space Flight Center, Earth Sciences Division, Greenbelt, Maryland, USA [4]Naval Research Laboratory, Monterey, California, USA, [5]Department of Mathematics, St. Edwards's University, Austin, Texas, USA.

Corresponding author: Joseph L. Wilkins (wilkins.joseph@epa.gov)

Key Points:

- Stratospheric intrusions can contribute 10 to 25 ppbv to the background ozone.
- Biomass burning plumes can contribute 10 to 80 ppbv to the background ozone.
- Biomass burning in the western U.S. can significantly increase Midwest pollution levels.

Abstract

Naturally occurring ozone rich Stratosphere-to-Troposphere Transport (STT) intrusions and biomass burning (BB) plumes reaching the surface can contribute to exceedances of the U.S. National Ambient Air Quality Standards for ground-level ozone (70 ppbv implemented in 2015). Additionally, fires can inject significant pollution into the free troposphere where it can be transported long distances. The combined air quality impacts from these sources on ozone has only been analyzed in a few case studies for the Midwest U.S. Here we study ozone impacts in a Midwestern city, for the first time in St. Louis, Missouri, using a series of ozonesonde profiles taken during the SEAC4RS (Studies of Emissions and Atmospheric Composition, Clouds and Climate Coupling by Regional Surveys) field campaign in August-September 2013. All ozonesondes showed enhancements above the background profile levels (~55 ppbv) throughout each tropospheric column. Two models were used to estimate ozone origins in columns. A chemical transport model identified STT enhancements equivalent to 10 to 15 ppbv over the background with a 10 to 15% contribution overall to the column. Two FLEXPART-WRF simulations, one with smoke in the boundary layer and another with smoke above, identified BB enhancements equivalent to 10 to 80 ppbv. Overall, the total BB contribution is 15 to 30% of the total column. Five ozonesondes showed signatures of mixed BB plumes and STT intrusions. During this study period, BB in the western U.S. contributed 70% to ozone enhancements in the total column compared to 3% from the central U.S and 27% from other areas.

Plain Language Summary

Because man-made emissions are decreasing, concentrations of harmful ozone pollution have also decreased in many areas of the USA. Not all sources can be easily controlled however. For example, biomass burning emits lots of pollutants to the atmosphere, and descending air from the stratosphere can bring with it high levels of ozone. These sources can pollute first the air above us, and then when the air is transported to the surface it can pollute the air we breathe. In this study we used balloons to measure ozone pollution as it changes from the surface to high in the atmosphere. We then used computer models to identify the sources responsible for higher pollution levels. Our study was part of a major field campaign that took place in the Midwest U.S. in the summer of 2013.

1 Introduction

Even moderate concentrations of ground-level ozone (O_3) can adversely affect human health and the environment across the United States (U.S. EPA, 2015). To lessen these impacts, the U.S. Environmental Protection Agency (U.S. EPA) has lowered the National Ambient Air Quality Standard (NAAQS) for O_3 from 75 to 70 parts-per-billion-per-volume (ppbv) (U.S. EPA, 2015). Ozone is a key secondary air pollutant associated with a large number of health issues ranging from asthma to premature deaths (Fann et al., 2013, 2018; Reid et al., 2016; Rappold et al., 2017), leading to 12,300 to 52,000 annual premature deaths in North America alone (Silva et al., 2013). Due to more stringent regulations over the past twenty years, regional ozone levels have declined by 7 to 13% (Simon et al., 2015; Strode et al., 2015). New evidence has demonstrated that even at lower concentrations ozone can still be very toxic (U.S. EPA, 2013). Despite overall progress, ozone concentrations may still be increasing in some areas (Fishman et al., 2014; Cooper et al., 2015; Jaffe et al., 2018), particularly in fire prone regions (McClure & Jaffe 2018).

Regulating locally formed ozone is complicated by the fact that ozone has significant background levels in the troposphere typically ranging 30 to 50 ppbv (Jaffe et al., 2018). Background concentrations of ozone can be enhanced due to noncontrollable ozone sources (NCOS), defined by Jaffe et al. (2018) to include recent local pollution influence from Stratosphere-to-Troposphere Transport (STT), lingering biomass burning emissions, long-range transport from international sources, lightning, or photochemical production from precursor emissions (e.g. nitrogen oxides and volatile organic compounds). Therefore, in this study we define background ozone to include NCOS. While foreign sources of pollution and wildfires are theoretically controllable, these are beyond the control of any local jurisdiction, so for this discussion, we can justify including these as background ozone. Over the past decade, significant progress has been made in our efforts to understand aspects of the U.S. background ozone problem for example: episodic stratospheric sources (Lin et al., 2015), interannual variability (Strode et al., 2015), and wildfire contributions (Jaffe et al., 2013; Westerling, 2016). However, these efforts have lacked coordination, and are largely focused on the impacts to the western U.S. where NCOS are considered to be the greatest (Jaffe & Wigder, 2012; Jaffe et al., 2018). Despite a 15 to 33% reduction in ozone precursors from anthropogenic emissions across the Eastern and Midwestern U.S. (Strode et al., 2015), the Midwestern background ozone levels continue to increase ~0.23 ppbv per year (Fishman et al., 2014) on par with the trends in the intermountain western U.S.

The Midwestern U.S., like the intermountain west U.S., is frequently impacted by biomass burning (McCarty et al., 2007; Liu et al., 2016) and stratospheric intrusions (Lin et al., 2015; Langford et al., 2018). Although biomass burning in the Midwest consists mostly of smaller agricultural fields, their combined emitted pollution and higher frequency can result in emissions double that of wildfires (Larkin et al., 2014). Understanding stratospheric intrusions and biomass burning contributions for this region will be critical as they can confound NAAQS attainment (e.g., Jaffe, 2011; Lin et al., 2012; Hess and Zbinden, 2013), where summertime daily ozone maxima already range from 70 to 80 ppbv and occasionally reach mixing ratios higher than 140 ppbv (Fishman et al., 2014). The periodic nature of some NCOS makes it difficult to target these sources with dedicated field campaigns, but opportunistic measurements have been made during field studies with other objectives (Sullivan et al., 2015; Ott et al., 2016). For

example, the influence of wildfires, long-range transport, and SST were the foci of the Las Vegas ozone Study (LVOS) where it was demonstrated that NCOS contributed ~30 ppbv to three ozone exceedances (Langford et al., 2015).

The SEAC4RS (Studies of Emissions and Atmospheric Composition, Clouds and Climate Coupling by Regional Surveys) field campaign in August-September 2013 presents a unique opportunity to study Midwest U.S. background ozone (Toon et al., 2016). During the flight mission several ozonesondes were launched nearly every day to measure vertical profiles of column ozone and meteorology over seven U.S. stations in a network known as SEACIONS (SouthEast American Consortium for Intensive Ozonesonde Network Study). The SEAC4RS campaign sparked a growing number of studies concerning ozone in the southeast U.S. (Travis et al., 2016; Wagner et al., 2015; Zhu et al., 2016). Although the research flights did not cover the Midwest U.S., this area is of interest because the time of the field campaign was an active period for NCOS with signatures for STT, large fires in the western U.S., and smaller prescribed fires in the central U.S. (~0.2 million hectares burned). During the 2013 ozone season (1 April through 31 October) fifteen total ozone exceedances occurred with six high-ozone days occurring during SEAC4RS. Additionally, a satellite-based detection method identified smoke plumes with confirmed injection heights above the boundary layer, initiated by smoke-infused thunderstorms known as pyrocumulonimbus or pyroCb (Fromm et al., 2010, 2019; Peterson et al., 2015, 2017a,b, 2018). The parametrization of plume rise from biomass burning can vary widely and cause undue biases and errors within model simulations of pollution transport (Paugam et al., 2016; Wilkins et al., 2018; Val martin et al., 2012, 2018). The detection algorithm used for the smoke plumes reduced the uncertainty of the injection heights and gave improved estimates based on remote sensing of each specific case.

Using a chemical transport model, it has been shown that fires can contribute ~14% to daily max ozone levels in the central U.S. (Wilkins et al., 2018). This has driven the need for developing accurate tropospheric ozone budgets for a typical summertime in the Midwest as suggested by Wilkins et al. (2018). Several approaches have been used to partition or identify the individual contribution of a naturally occurring ozone rich STT intrusions (Langford et al., 2018), a biomass burning plume (Westerling, 2016), or their combined impacts (Brioude et al., 2007) to elevated ozone levels. These approaches include the use of intensive balloon-borne ozonesonde field campaigns (Cooper et al., 2007; Thompson et al., 2019); lidar and aircraft remote sensing (Brioude et al., 2007; Langford et al., 2018); and Lagrangian trajectory and chemical transport models (Morris et al., 2006; Baker et al., 2016, 2018). However, the determination of the contribution from individual sources to local ozone enhancement with a single point measurement remains difficult (Thompson et al., 2019), and it can be even more challenging to quantify accurately the contribution from multiple sources (Lin et al., 2015). In particular, the partitioning of these sources is critical for NAAQS attainment investigations along with long-term trend determinations, as they are two of the most critical NCOS imported (Parrish et al., 2012, 2014). Further, 30% of the present-day atmospheric ozone burden is attributable to human activity and these emissions are still rising (Granier et al., 2011; Parrish et al., 2010). For example, Li et al. (2019) using ~1,000 surface ozone sites over a five year period (2013-2017) showed that East Asian concentrations are continuing at +1 to 3 ppbv per year. In this study, we use ozonesonde measurements from the SEAC4RS campaign and models to identify and characterize contributions from biomass burning and stratospheric intrusions to tropospheric ozone columns above the Midwest background ozone levels. Additionally, we evaluate the

contribution from fires observed in the western and Midwest U.S. to ozone concentration in St. Louis.

2 Tropospheric Ozone and Meteorological Soundings

Vertical profiles of ozone, pressure, humidity, and temperature were measured using balloon-borne ozonesondes coupled with radiosondes. Each ozonesonde consists of a Teflon pump, an ozone sensing electrochemical concentration cell (ECC) (Komhyr et al., 1986, 1995), attached alongside a Vaisala RS-8015N radiosonde. The instruments were prepared in accordance with the Southern Hemisphere Additional Ozonesondes (SHADOZ) protocol (Thompson et al., 2011a,b, 2019). The ECC-type ozonesonde is currently the most widely used due to its well-characterized behavior and working capability under various sky conditions (Kuang et al., 2012). Comparisons with other O_3 measuring instruments have demonstrated the ECC sonde precision to be ±5% near the ground and ±10% in the upper troposphere, although errors can reach 17% (Thompson et al., 2007; Stauffer et al., 2014). The radiosonde temperature and pressure sensors have accuracies below 20 km of ±0.3°C and ±0.5 hPa, respectively (Lal et al., 2014). The heights were calculated based on the observed pressure and are above sea level (asl). The humidity sensor has an accuracy of about ±2% near the ground which decreases to ±15-30% in the 5 to 15 km altitude range (Kley et al., 1997; Hurst et al., 2011).

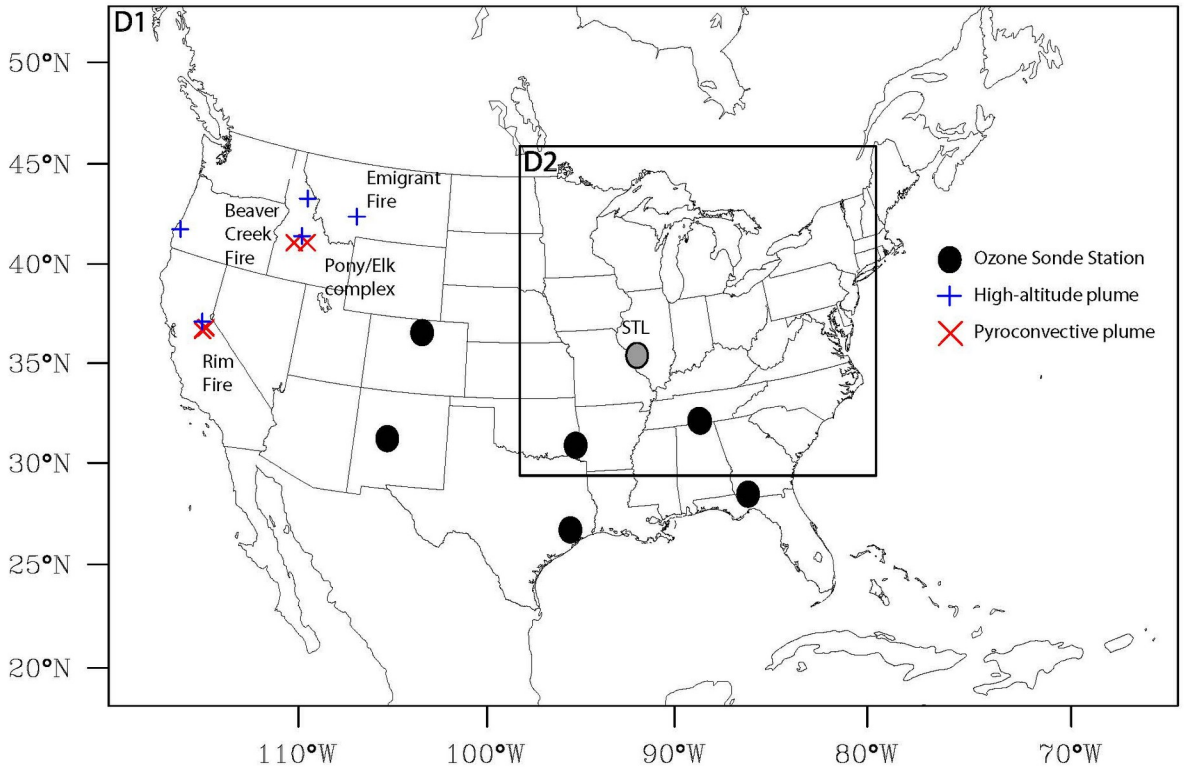

Figure 1. Study area map with FLEXPART-WRF model domain. Rectangles mark the WRF domains D1 which has a horizontal resolution of 12 km and D2 (4 km resolution). SEACIONS locations are marked by black circles (St. Louis, Missouri station (STL) is a gray circle). Wildfire emissions from FLAMBE, August-September 2013, with eleven Pyro convective and

five high-altitude injection elevated smoke plume activity areas are marked, red crosses indicate pyroCb plumes which transport smoke into the upper troposphere and lower stratosphere. Blue crosses indicate high-altitude injection of smoke in the absence of large pyroCb which transport smoke into the mid-troposphere).

Figure 1 displays the seven ozonesonde sites across the U.S. for the South East American Consortium for Intensive Ozone Network Study (SEACIONS) — archived at http://croc.gsfc.nasa.gov/seacions/. Here, we focus on the sole midwestern U.S. site located at the James S. McDonnell Planetarium in Forest Park (90.27W, 38.63N, 181 m ASL), ~5 km west of downtown St. Louis, Missouri. Balloon soundings carrying an ozonesonde and a radiosonde were made near daily between 10:00 to 14:00 (UTC - 5 h). The exact launch time depended on clearance from the Air Traffic Control of the local airport and weather conditions. The first flight was made on 8 August 2013 and the last on 22 September 2013. There were breaks scheduled between the launches in order to cover the time period of the larger SEAC4RS flight mission (Toon et al., 2016). A total of 28 ozonesondes were launched during this period from St. Louis. The balloons reached a maximum altitude of 22 to 36 km with an average ascent rate of about ~5 ms^{-1}. The instruments fell mostly within 70 km of the launch site.

Vertical curtain plots of ozone concentrations are shown in Figure 2, displayed in 500 m bins up to 15 km height. The figure shows structures in the tropospheric ozone profile which will be analyzed for impacts of stratospheric air masses and biomass burning sources using the modeling techniques demonstrated by Thompson et al. (2007, 2011b).

3 Numerical Models

3.1. Stratospheric-to-Tropospheric Transport ozone tracer model

To simulate the stratospheric air masses entering the troposphere during the SEACIONS field campaign, the NASA Goddard Earth Observing System model (GEOS-5, Rienecker et al., 2008) was used. The model analysis was provided on 72 levels from the surface to 0.01 hPa (~75 km), every 6 hours. Initial conditions for the atmospheric component were taken from uncoupled experiments forced by the observed sea surface temperature. The model defines a stratospheric intrusion as air masses with a high ozone composition, potential vorticity greater than 1.5 potential vorticity units (PVU; 1 PVU = 10^{-6} m^2 s^{-1} K kg^{-1}), and a relative humidity (RH) of less than 20% (e.g. Holton et al., 1995; Waugh and Funatsu, 2003; Stohl, 2003). Here we categorize each STT by temporal duration, vertical extent, and meteorological cause and relate them to the contributions to the tropospheric ozone column. Previously, GEOS-5 has been used extensively for stratospheric intrusions and has been validated with ozonesonde observations (e.g. Stajner et al., 2008; Wargan et al., 2015). A review of data assimilation methodology applied to chemical constituents, including ozone, can be found in Lahoz et al. (2007).

3.2. Dispersion Model

3.2.1. FLEXPART-WRF Lagrangian Dispersion Model

The FLEXPART-WRF version 3.1 (Brioude et al., 2013) was used as a Lagrangian particle dispersion model using wind fields from the Weather Research and Forecasting (WRF version 3.4, Skamarock et al., 2008). Simulations were made for seven days to relate

ozonesonde profiles to biomass burning events. FLEXPART-WRF was used to simulate carbon monoxide (CO) as a passive tracer for biomass burning plumes. The plume injection heights were adjusted to match the impacts with the vertical ozone profiles at a resolution of 100 m. The model does not include chemical loss or production in its trajectory calculations. The simulations can be used to estimate CO concentrations using multiple particles each representing a fixed amount of CO emitted and transported as a passive scalar. Therefore, trajectories aged 5 to 15 days can be considered as mixing ratios above background (Brioude et al., 2007). WRF was initialized using the North American Regional Reanalysis (NARR, Mesinger et al., 2006) wind fields, with hourly temporal resolution, two nested domains with a horizontal resolution of 27 km and 9 km, and 40 pressure levels. Figure 1 shows a map of the two nested WRF domains. Nine individual WRF simulations were performed to cover the entire time span of the SEACIONS mission. Each simulation lasted 162 h with 42 h of spin-up time and the remaining five days were used for the analysis (de Foy et al., 2014).

To determine the transport impacting each ozone measurement, a plume origin path was calculated. The plume path was determined based on several thousand forward trajectory particles released from a box surrounding the location and time of biomass burning present over the 44 day period. Plume origin path distributions were output in 1 day intervals on a 2.5˚ x 2.5˚ output grid at 500 m vertical resolution covering the U.S., with a 0.25˚ x 0.25˚ at 100 m vertical resolution nested grid over St. Louis. FLEXPART-WRF outputs the plume origin paths in units of s kg^{-1} m^3, which represents the residence time of the plume per grid cell divided by the air density. The residence of each plume was calculated for the surface to upper troposphere (~0 to 15 km) layers of the atmosphere. This is known as a weighted plume residence time (Lal et al., 2014).

The dispersion of a plume origin path forward in time indicates the likely source regions contribution of the ozone precursors to the measured ozone but over the previous 7 days. For plumes passing through these layers, the residence time of the forward trajectories can interact with stratospheric intrusions allowing for the detection of mixed plumes. Hourly biomass burning emissions were provided by the Fire Locating and Modeling of Burning Emissions (FLAMBE) program (http://www.nrlmry.navy.mil/flambe/) (Reid et al., 2009). The emission factors are outlined by Ferek et al. (1998). FLAMBE provides quasi-operational, with fire location, instantaneous estimates of fire size, and smoke emission flux in kg m^{-2} generated in near real time for the Western Hemisphere (Reid et al., 2009). The inventory uses active fire detection from the GOES's Wildfire Automated Biomass Burning Algorithm (WF-ABBA) and MODIS's Active Fire Products to detect biomass burning activity in near-real-time (Reid et al., 2009). The fire emissions are calculated in grams of CO from the inventories' burned area (m^2) and smoke aerosol emissions (CO in gm^{-2}) variables. The fire emissions are mapped onto a 0.25˚ x 0.25˚ grid as input to FLEXPART-WRF. With this technique, the quantity of CO emitted into each plume from several fire source regions across the U.S. was tabulated. The CO tracer has no chemical or depositional removal processes and was treated as a passive tracer. The NARR analysis contains information that can be used to derive stratospheric ozone values above and within the troposphere. We used these values to calculate the quantity of ozone transported from the stratosphere to the location where a plume was released. NARR provides more information on the stratospheric intrusions structure with temporal coverage 8-times daily and a 32 km spatial grid. Stratospheric intrusions in NARR were calculated using PVU distribution on isentropic surfaces, 320 K to 410 K (≈ 80 hPa). Specifically, with NARR we can closely match ozonesonde

launch times with meteorological data (~18:00 UTC); this allows for better comparison with model and observed stratospheric intrusions.

3.2.2. FLEXPART-WRF high-altitude smoke injection

To account for the vertical extent (or plume injection height) of varying biomass burning emissions in the simulations, we employ the FLEXPART-WRF model. The BASELINE simulation represents biomass burning emissions as a uniform release within the well-mixed boundary layer up to ~3.5 km (e.g. Liousse et al., 1996; Colarco, 2004; Davison, 2004; Brioude et al., 2007). To represent plumes that penetrate well above the boundary layer, we use the U.S. Naval Research Laboratory (NRL) satellite-based pyroCb detection algorithm and inventory (Peterson et al., 2017a,b) — referred to hereafter as the PYRO simulation. For a confirmed pyroCb, the plume tops are set at the model determined Upper Troposphere and Lower Stratosphere (UTLS) boundary (~9 to 15 km). For non-pyroCb, plume tops are set to be near the model determined middle troposphere (~5 km). In both cases, the plume bottoms are set above the PBL, with the emissions uniformly distributed within the tropospheric model layers. Lastly, a method is presented that is a combination of the two methods mentioned above (BASELINE + PYRO) referred to hereafter as the combined method. The combined method was run as a single simulation and compared to each individual method. The combined simulation included all the emissions from the Baseline, with addition of the elevated emissions from the fires with pyro convective plumes identified in Figure 1, see Table 1 for more details.

Peterson et al. (2017a) examined a variety of wildfires and pyroconvective events in western North America during the summer (June to August) of 2013. At least 26 intense pyroCb events were inventoried, injecting smoke particles well into the UTLS. Several fires produced smaller pyroCbs and others injected smoke above the boundary layer in the absence of significant pyroCb activity (Figure 1). The NRL pyroCb detection algorithm is designed to detect large plumes that impact the UTLS, and in general, is not designed to capture lower tropospheric transport. The algorithm only detects anvil cloud tops; therefore, neither the exact quantitative plume height nor a plume bottom can be detected.

A variety of additional observations and methods exist to track the evolution of pyroCb smoke plumes in the UTLS after the initial injection (e.g., Fromm et al., 2010, 2019; Peterson et al., 2018). However, application of these methods is beyond the scope of this study. Evolution and transport of significant pyroCb plumes from the 2013 fire season are examined in greater detail by Peterson et al. (2015, 2017a,b) and Fromm et al. (2019).

4 Results and Discussions

4.1. The structure of tropospheric ozone columns

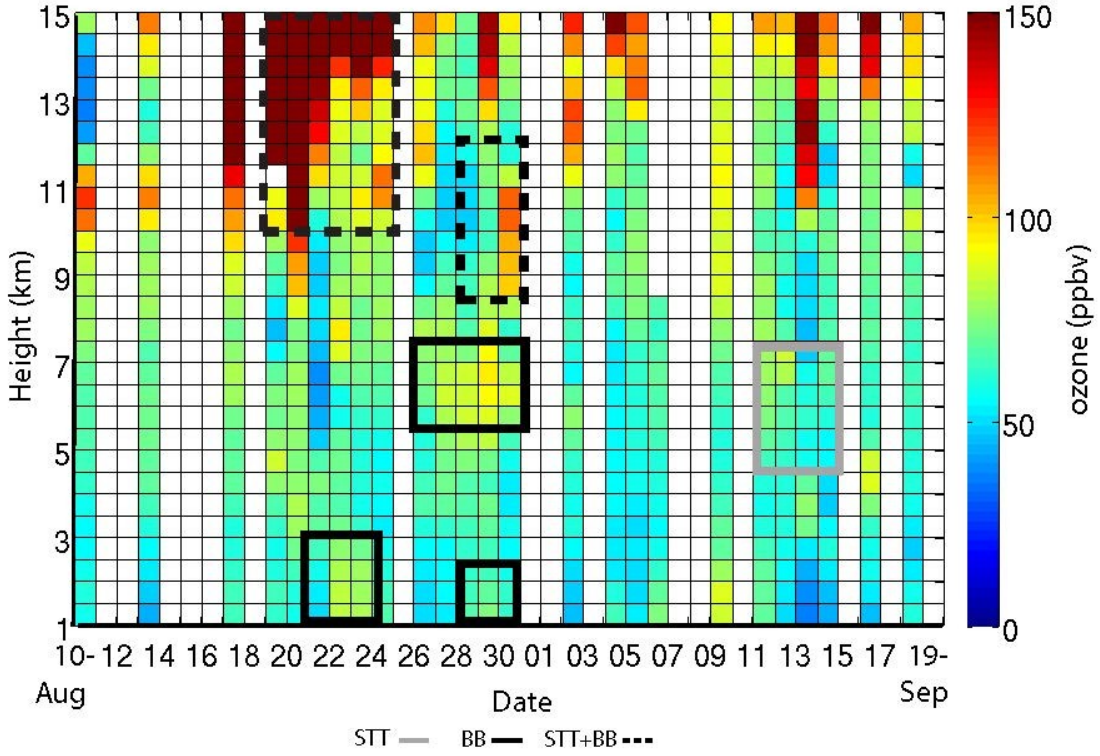

Figure 2. Ozonesondes in support of SEACIONS were launched at the Saint Louis University ozonesonde station located at the James S. McDonnell Planetarium in Forest Park (90.27˚W, 38.63˚N, 181 m asl), 5 km west of downtown St. Louis. Vertical tropospheric profiles at ~18:30 UTC (1:30 p.m. Local time) ozone profiles are averaged vertically every 500 m and shown below the thermal tropopause level (~15 km). Cases of ozone enhancements above the background (~55 ppbv) are shown by source origin: the gray box for Stratospheric-Tropospheric Transport (STT), the solid black line boxes for biomass burning (BB), and the dashed line black boxes for combined STT and BB.

The vertically averaged near-daily profiles of ozone are shown in Figure 2. The profiles are averaged every 500 m vertically from the surface to the tropopause (~15 km) with annotations for enhanced ozone rich plumes, above the tropospheric column mean (55.7 ppbv), from biomass burning and stratospheric intrusions. Ozone gradually increases with altitude in the lower troposphere (below about 3.5 km). Average ozone is about 55 ppbv near the surface but decreases to 45 ppbv near 3.5 km. Above 3.5 km, ozone increases slowly throughout the entire troposphere a rate of 3 ppbv km^{-1}. In the middle troposphere (4 to 10 km, height), average ozone is highest in August and lowest in September. While above 10 km, ozone is similar for both months. August profiles averaged 10 to 15 ppbv higher than September. Ozone is lowest (~40 ppbv) during the month of September near the surface and remains low below 3.5 km. However, on 5 September the second highest recorded surface ozone day occurred at the surface (60 ppbv ozonesonde, 95 ppbv nearby surface monitor later in the day). The maximum measured ozone

from a sonde at the surface occurred 30 August at 65 ppbv. Other notable enhancements (NAAQS exceedances) of O_3 (> 70 ppb near the surface) occurred on 23 August, and 4 to 6 and 10 to 11 September. A mean PBL of 2.4 km and a mean thermal tropopause at 14.9 km could be clearly identified in the ozonesonde profiles. Note that these figures for biomass burning contributions from boreal fire contributions to ozone downwind are somewhat larger than the 5 to 15% estimates of this quantity by Thompson et al. (2011; see Figure 13) or Moeini et al. (2020) that are based on Canadian soundings. These last two studies attribute 20 to 25% of the ozone column amounts to stratospheric origins.

4.2. Stratospheric-tropospheric transport tracer impacts

Table 2 lists the GEOS-5 determined stratospheric instructions events that impacted St. Louis during August and September 2013, expressed as deep or shallow with the pressure level 600 hPa being the threshold. The 44 day study period consisted of 13 events. The intrusions recorded resulted from either a shortwave trough (6 days: 7, 10, 23, 28, 30 August and 6 September), frontal passage (7 days: 3, 12 August and 3, 12, 15, 22 September), or cut-off low (1 day: 14 August). Three frontal pass intrusions reached the lower troposphere and penetrated the boundary layer. About 40% of the intrusions reached the middle troposphere (~500 hPa). Stratospheric intrusion generally lasted 1 to 3 days occurring either early morning before 3:00 (UTC – 5 h) or around noon local time. The intrusions where found to contribute on average 10 to 25 ppbv to tropospheric ozone columns which equates to around 5 to 15% of the total tropospheric ozone column.

4.3. Biomass Burning Emissions

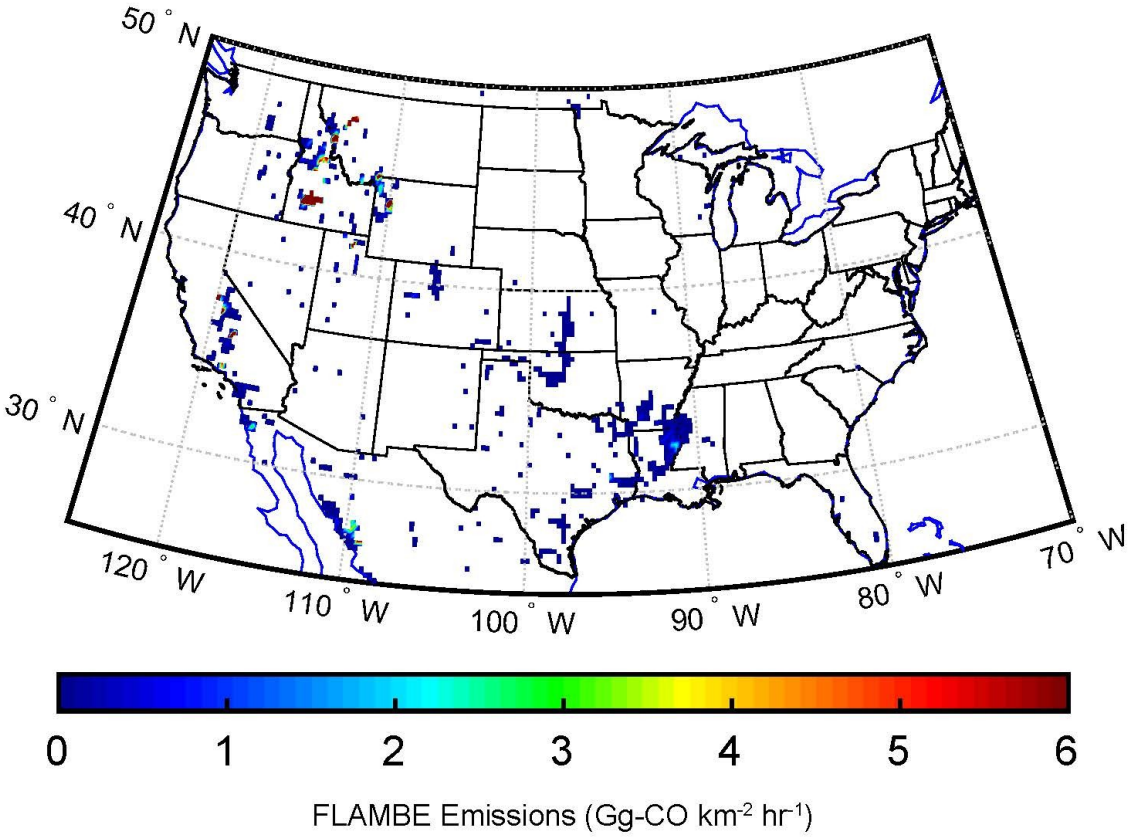

Figure 3. Biomass burning emissions of carbon monoxide (CO) estimated by FLAMBE in units of Gg per km^2 per hour in North America during SEACIONS, 8 Aug to 22 Sept 2013. FLAMBE emissions are displayed on the model grid which has a resolution of 0.25˚ per cell. Only cells with emissions above 2,000 kg are shown.

Figure 3 shows the hourly U.S. total mass of fire smoke emissions from FLAMBE in Gg-CO km^{-2} hr^{-1} gridded per 0.25˚ cell with a minimum threshold of 2,000 kg. From 8 August to 22 September 2013 the calculated total emissions were 1,060 Gg of CO. FLAMBE emissions depict a regional distribution pattern in known fire regions: agricultural and prescribed fires in the southeast U.S. (e.g. the Carolinas, Florida, and Georgia) and southcentral U.S. (e.g. Louisiana, Mississippi, and Arkansas); and the wildfires in the central plains and intermountain west U.S. (e.g. Wyoming, Idaho/Montana area, and California). A time series of the hourly emissions indicates that August contained almost all the major fire emissions (Figure 4). The duration of the largest fire emissions are indicated in the figure by arrows. Between 14 and 24 August 2013, on average ~6 Gg-CO hr^{-1} (~1.2 x 10^4 FLEXPART particles where 1 particle = 500 kg = 0.5x10^{-3} Gg) was being emitted daily with a maximum hourly total of 11 Gg-CO hr^{-1} (~2.2 x 10^4 FLEXPART particles). Regional fires emissions from the central U.S. were considerably lower than wildfires emissions in the intermountain west (3% compared to 70%).

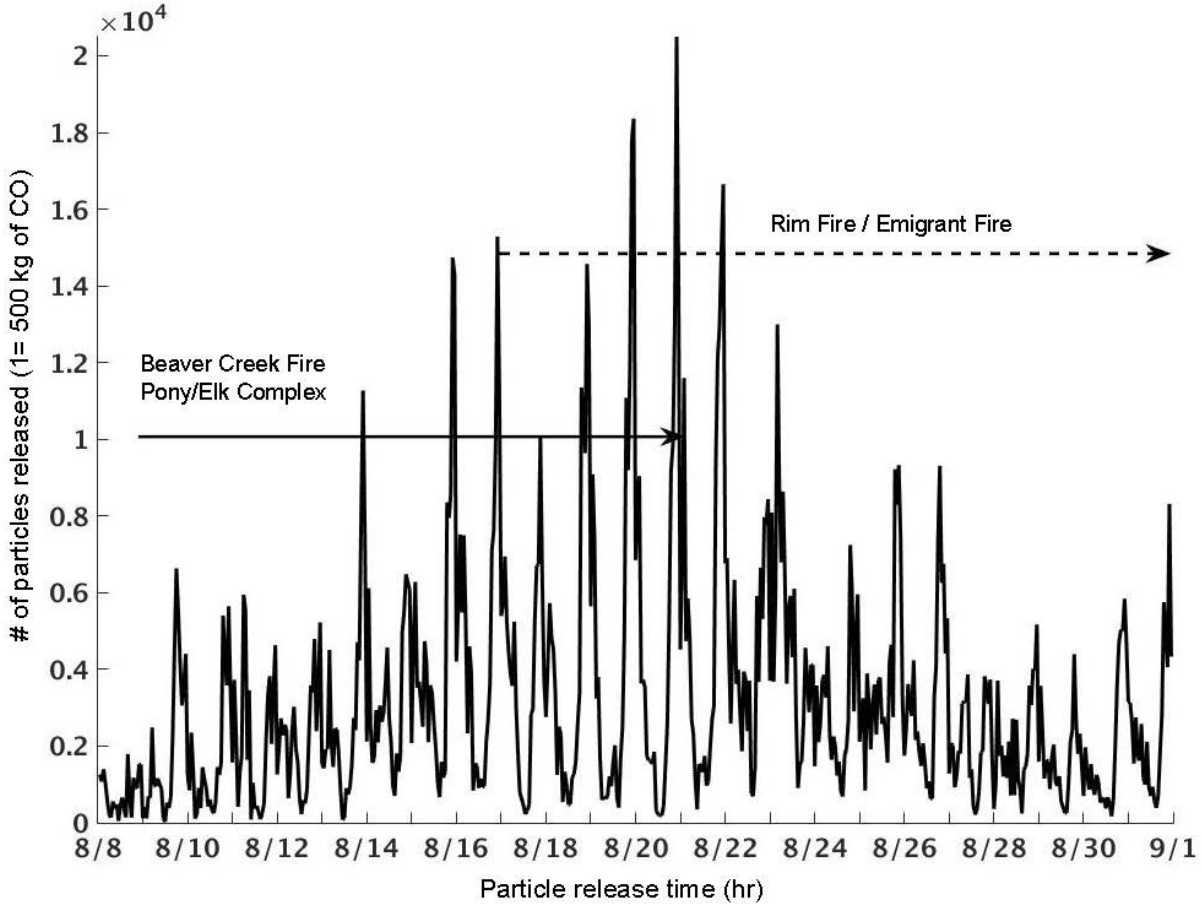

345 **Figure 4.** A time series of FLAMBE emissions (mass/time) converted to particles released in
346 FLEXPART-WRF (# of particles or particle count). Each 500 kg of mass is converted to 1
347 particle in FLEXPART-WRF simulations. Locations emitting less than 500 kg only emit a single
348 particle. Arrows represent the duration of two of the largest wildfires (Rim Fire and Beaver
349 Creek) with relevance to SEACIONS with other fires (Emigrant Fire and Pony/Elk Complex)
350 contributing to those time frame emissions indicated. The dotted line is the California Rim Fire
351 (37.85˚N, 120.083˚W) 17-31 August 2013, and the solid line is the Idaho Beaver Creek
352 (43.593˚N, 114.684˚W) 7-21 August 2013. Note: Beaver Creek and Pony/Elk Complex occurred
353 nearly at the same time and were fewer than 100 km apart in distance. While, the Emigrant Fire
354 contributed a significant amount of emissions during its occurrence at the same time as the Rim
355 Fire but was much smaller in magnitude.
356

357 Specifically, three large wildfires areas were identified that produced the most emissions
358 and high-altitude smoke injection plumes. The Idaho Beaver Creek fire, caused by a lightning
359 strike on 7 August 2013 in the Sawtooth National Forest, occurred in the lower southwestern
360 edge of the Elk/Pony Complex (43.59˚N, 114.68˚W). This fire burned an area of 465 km^2
361 (114,900 acres), emitting 54.6 Gg-CO of smoke emissions, and accounted for 14% of the Idaho
362 and Montana states combined total fire emissions (392 Gg-CO km^{-2} hr^{-1}) during the months of
363 August and September. The second fire area, led by a fire named the Montana Emigrant Fire,
364 was a part of a small system of fires caused by multiple lightning strikes that spanned across
365 Yellowstone National Park (45.20˚N, 110.69˚W) consuming <81 km^2 (20,000 acres) starting 14
366 August emitting 9.4 Gg-CO of smoke emissions. Lastly, the largest of the three, the California
367 Rim Fire, described in detail in Peterson et al. (2015), caused by an illegal campfire, occurred on
368 17 August 2013 in Yosemite National Park (37.85˚N, 120.08˚W). The Rim Fire burned an area
369 of 1041 km^2 (257,314 acres), emitted 224 Gg-CO of smoke, and accounted for over 66% of the
370 California biomass burning emissions (341 Gg-CO km^{-2} hr^{-1}) during SEAC4RS.

371 4.4. Residence time of particles over St. Louis

372

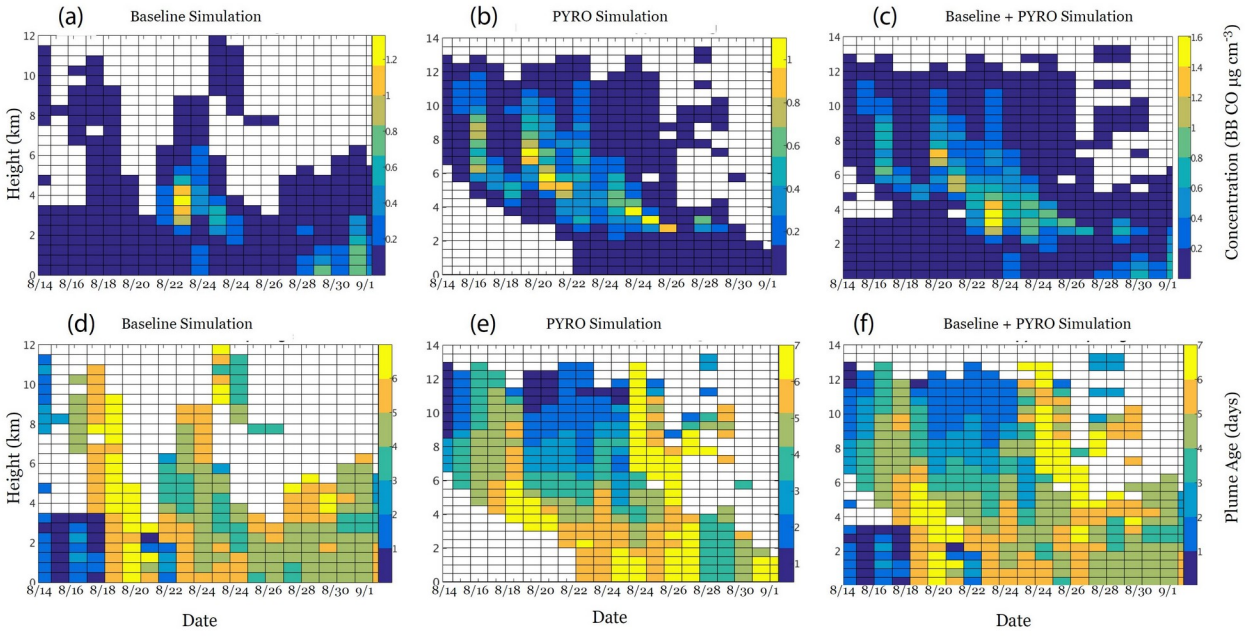

373

374 **Figure 5.** FLEXPART-WRF Biomass burning (BB) CO concentrations and age are simulated,
375 binning trajectories over St. Louis within a 2.5˚ x 2.5˚ grid box and averaged vertically 500 m
376 with daily temporal resolution. FLAMBE emissions of BB CO are converted into particle
377 amounts and are released. (a) The base simulation, Boundary Layer Simulation, releases
378 emissions within the PBL, (b) NRL's adjusted pyro-convention scheme is implemented, PyroCb
379 Simulation, particles are released from pyroCbs and high-altitude injection as specified in Table
380 1, and (c). The combined (a) and (b). With panels (d-f), corresponding to plume ages in
381 simulations. The average BB CO g cm^{-3} per grid cell (top) lighter shading indicated higher
382 concentration and transported CO plume ages (bottom) lighter shading indicates older air.

383

384 The FLEXPART-WRF plume origin path (forward trajectories) has been used to
385 calculate residence times of air parcels above St. Louis (Figure 5). Figure 5a-5f show the average
386 residence times of the biomass burning plume origin paths expressed as plume age and CO tracer
387 particle amounts as concentrations. Results are displayed for the BASELINE simulation (Figure
388 5a and 5d), PYRO simulation (Figure 5b and 5e), and combined (Figure 5c and 5f). The lighter
389 shading represents a higher concentration of CO particle counts (Figure 5a-5c) and for plume age
390 the lighter shading indicates older air (Figure 5d-5f). The major contributions below 3 km are
391 from the central U.S. fires. The contributions from the intermountain west U.S. fires dominates
392 above 3 km, in the range of 80 to 90%. Other regions contribute in the range of 5 to 10%.
393 Biomass burning plumes are indicated to have impacted the surface ozone each day but with
394 varying magnitudes. The surface impacts were connected to mechanisms causing air parcels to
395 move downward (e.g. shortwave on 30 August). Likewise, strong vertical motion was evident in
396 bringing simulated air within the boundary to the middle and upper portions of the troposphere.

For example, on 24-26 August at the 8 to 12 km layer, both simulations indicate enhancements of 0.74 ppm of CO that has been aged ~7 days. This enhancement corresponded to ~40 ppb of excess O_3 at the 11 to 12 km layer in the ozonesondes. Ozone impacts for August from biomass burning, sharply increase after 3 km and vary daily above; up to 12 km where the biomass burning contributions to ozone decrease to near negligible amounts. The high-altitude smoke injection simulation indicates that plumes that get injected above the 4 km height can impact the surface. Evidence of aged lofted air, ranging from 4 to 15 km, impacting the surface is seen 22 August to 1 September 2013, where a constant ~2 ppm of CO enhancement at the surface is present. Additional evidence of biomass burning emissions enhancing ozone within the lower tropopause and PBL (0 to 6 km) is present on 21-24 August over the St. Louis area — a greater than 15 ppbv enhancement of ozone within a 6 day aged plume containing an additional 9 ppm of CO.

The average plume age for the August month ranged between 4 to 7 days. Plumes reaching the lower troposphere (below 3.5 km) were ~3 days fresher then plumes above. The simulated high-altitude smoke injection is typically ~2 days fresher than the boundary layer injected smoke when above 3 km but can be 2 days older when below. The average aged plume lead to 15 ppbv increase in ozone. As plumes aged, they became more ozone enriched. Fresher plumes have higher levels of CO but lower amounts of ozone. An example of this occurred 23 August, where and ozone exceedance at the surface was indicated in both simulations to be from a polluted air mass layer with mixed ages. From the lower and middle troposphere (below 1.5 km and above 5.5 km) the plumes ages averaged 2 days older, with about 7 ppm fewer CO, and 20 ppbv more ozone than the air in the layers in-between.

4.5. High-altitude smoke injection analysis

The impacts of high-altitude smoke injection are demonstrated using two examples from commonly encountered summertime synoptic meteorological situations in the central U.S. (i) cyclonic flow or a system of low pressure (e.g. cut-off low 17-21 August) and (ii) anti-cyclonic flow or a system of high pressure (e.g. blocking high 25-30 August). Table 3 lists each episode's ozone enriched plume identified by an ozonesonde over St. Louis (Figure 2). For each identified ozone enhancement, the simulated source-contribution relationships from biomass burning (Table 1) and stratospheric intrusions (Table 2) are quantified. The corresponding travel time of the plume (or plume age) and concentrations are indicated by FLEXPART-WRF (Figure 5). St. Louis area for two selected days (21 and 30 August). Each plume was individually characterized with model simulations and ozonesonde observational data in addition to the meteorological conditions leading to the plume reaching St. Louis is discussed below.

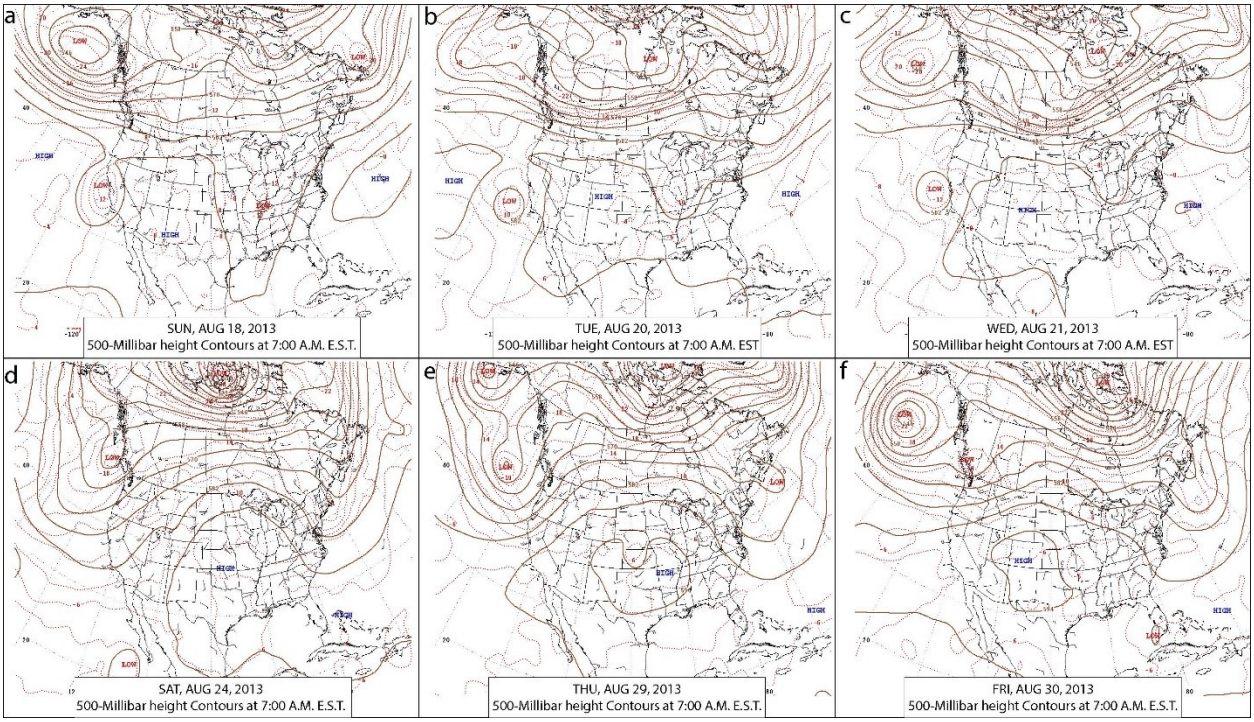

Figure 6. Series of daily synoptic atmospheric plane slices at 500 hPa at 7:00 UTC for preceding conditions to individual transport cases (a-c) 21 August 2013 (d-f) 30 August 2013.

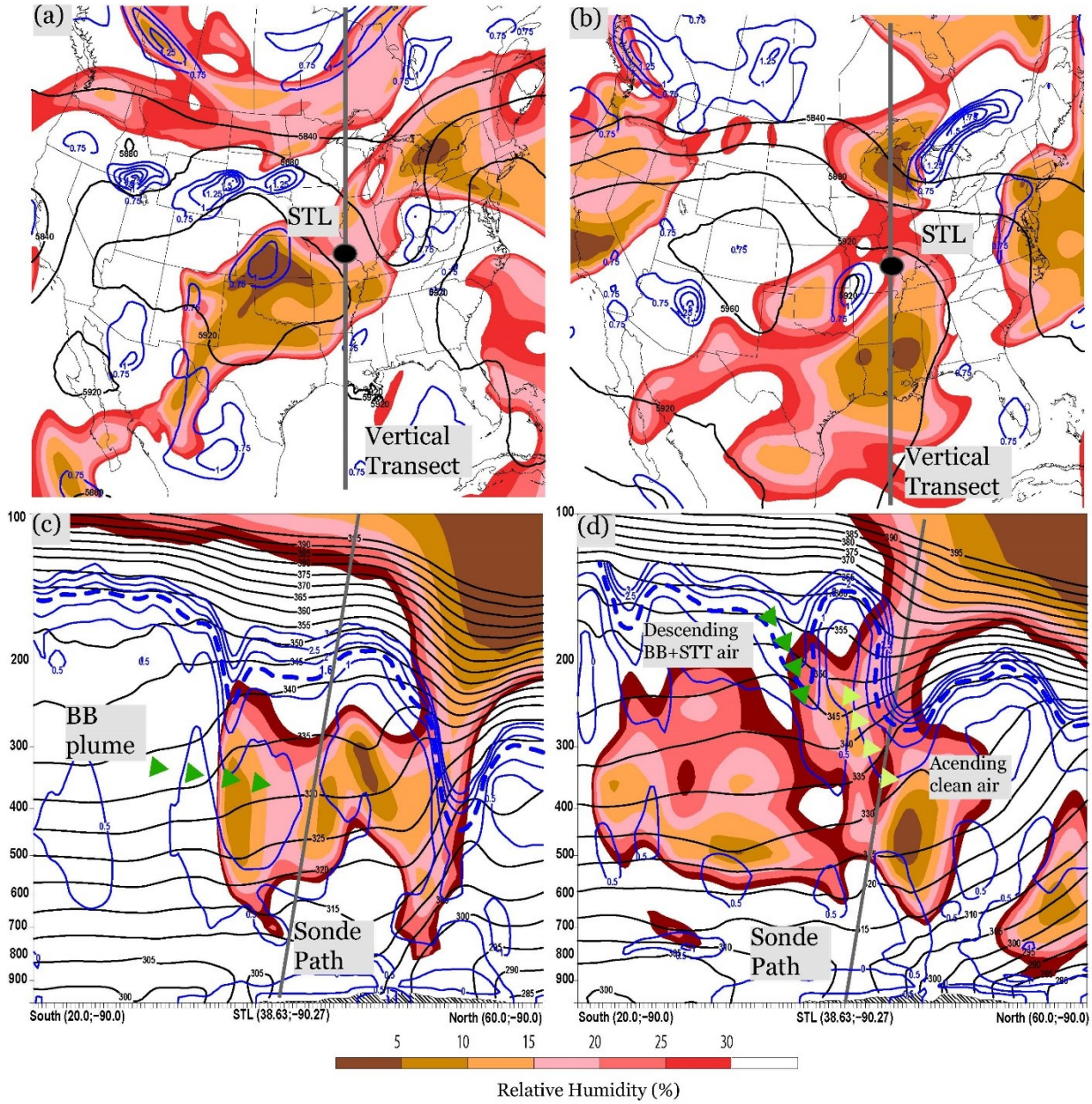

Figure 7. Atmospheric plane slices from NARR at 500 hPa at 18:00 UTC (a) 21 August 2013 (b) 30 August 2013. Vertical Cross sections at 90˚ W, 20-60˚ N 18:00 UT (c) 21 August 2013 (d) 30 August 2013. Blue contour lines show Potential Vorticity (PV) 10^6 PVU, Relative Humidity (RH) below 30% is shaded from light to dark, with darker shades representing the dryer air. The black lines on (a) and (b) are pressure height contours in m. While, the black lines on (c) and (d) represent potential temperature (isentropic surfaces) in K. Biomass burning sources tend to have low PV and can have moderate RH levels for pyroCbs, while stratospheric air masses have high PV and low RH. The blue dashed line PV contour (1.5 PV) shows the approximate boundary between stratospheric and tropospheric air masses. Arrows (green) show air-mass transport patterns from Stratospheric-Tropospheric Transport (STT) and from Biomass Burning (BB).

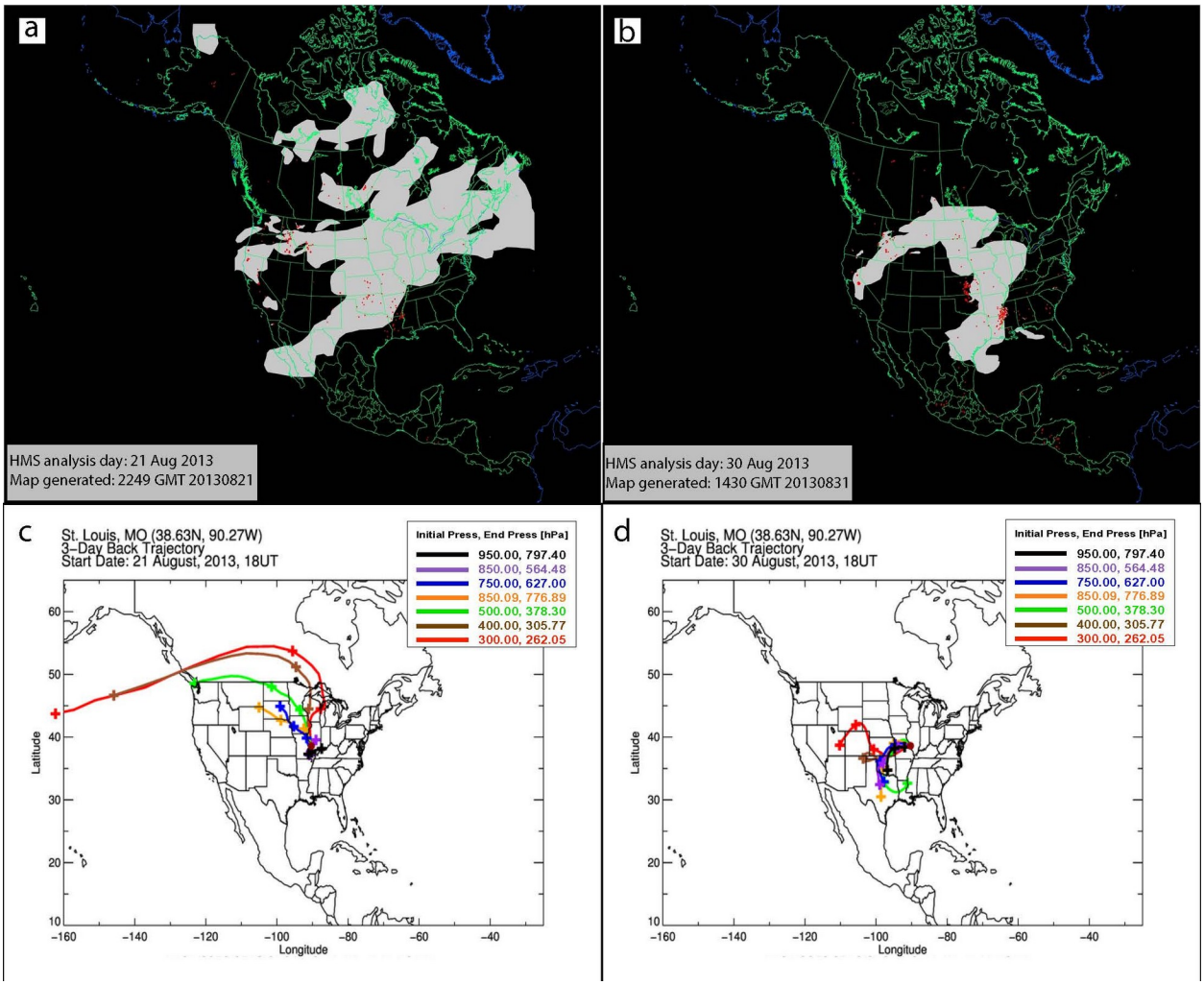

Figure 8. NOAA Hazard Management System (HMS) and Smoke Product analysis of smoke (a) 21 Aug 2013 and (b) 30 Aug 2013. Below, three-day backward FLEXPART-WRF trajectories corresponding to each episode is provided (c) 21 Aug 2013 and (d) 30 Aug 2013. Additional trajectories are placed in the data archive at https://tropo.gsfc.nasa.gov/seacions/.

4.5.1. 17-21 August 2013: Evidence of biomass burning advected by a cutoff low

The meteorological map provided in Figure 6a-c indicates biomass burning transported by a cut-off low originating on 17 August 2013 00:00 UTC at 500 hPa over central Missouri. In this case the cut-off low was created by a closed upper-level low pressure system that was cut off from a westerly current (14 August 06:30 UTC) and it began moving independently. The cut-off low remained nearly stationary until 19 August 00:00 UTC, at which time the trough filled in and moved eastward. Due to the nature of the quasi-stationary system, the westerly flow of air propagated the western fire plumes over the central U.S. and southeast U.S. Figure 7a and 7c present a cross section and plane view of the resulting low. Due to the low pressure system the trajectory analysis indicated that smoke flowed from various fire locations to the St. Louis area

(see Figure 8). Figure 9a-c depicts the vertical ozone and meteorological profiles representative of this time period (21 August). Refer to Figure 2 for corresponding ozonesonde curtain plots.

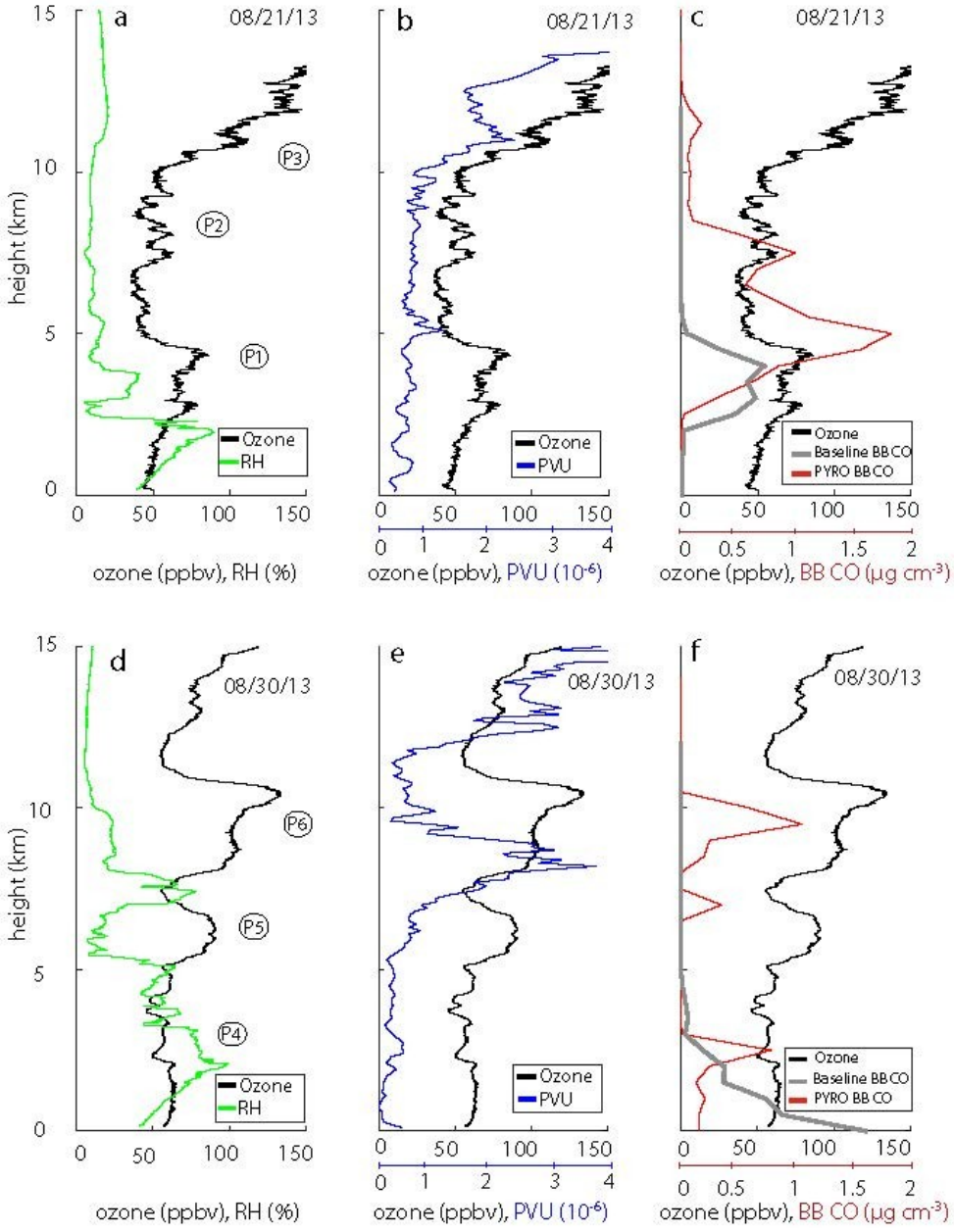

Figure 9. Vertical tropospheric profiles over St. Louis at ~18:30 to 19:30 UTC for selected test cases 21 August 2013 and 30 August 2013. Labels P1 to P6 correspond to plume information in Table 3. Ozone measured from the ozonesonde in ppb are shown as a black line. Panel (a) and (d), the green line RH %. Panel (b) and (e), the blue line represents the GEOS-5 modeled Potential Vorticity 10^6 PVU. Panel (c) and (f), the FLEXPART-WRF modeled CO biomass burning g cm^{-3}, for each simulation the PYRO simulation is red, and BASELINE simulation in gray. Refer to Figure 2 for corresponding ozonesonde curtain plots.

Three ozone enhanced layers are visible on 21 August (Table 3, Figure 9). None of these enhancements are deemed of stratospheric origins, as there was no significant PVU present in these layers. Plume P3 at 11 km was initially considered to be a stratospheric intrusion related but are ruled out as the NARR data and sonde thermal tropopause indicate that the tropopause was lowered (15 km to ~9 km) possibly by wave breaking from the cut-off low. The lower- and upper-middle tropospheric ozone enhancements at P1 (2 to 5.5 km) and P2 (7 to 9 km), respectively, are determined to be of biomass burning origin. The lower-tropospheric plume P1 was determined to be from the Idaho Beaver Creek plume ~6 days earlier. The upper-middle tropospheric plume P2 originated 2 days prior from high-altitude injection plumes from the Yellowstone National Park Emigrant cluster fires. The contribution of 21 August tropospheric ozone layers from biomass burning was 10 to 25 ppbv. The pyroCb from the Idaho Pony Elk Fire (16 Aug at 23:41 UTC) reached the St. Louis area; But, the polluted air remained in the lower stratospheric air and did not mix with the lower layers. The incorporation of the high-altitude injection plumes allowed for the two middle- and upper- tropospheric polluted plumes to be characterized which contributed ~15 to 30% to layers in the total ozone column. This upper level pollution was later advected down to the surface and contributed to the exceedance on the 23 August.

4.5.2. 25-30 August 2013: Evidence of stratospheric air mixing with aged biomass burning during anticyclonic flow

The meteorological map provided in Figure 6d-f indicates aged biomass burning transported into a stratospheric intrusion by a high pressure system that became well-established over Missouri 25 August 00:00 UTC. The high pressure system began developing a week prior over the southcentral U.S. The high remained quasi-permanent as it sat over Missouri reaching its maximum strength on 26 August 06:00 UTC until a mid-level (500 hPa) shortwave trough moved into the area on 29 August 12:00 UTC moving the system eastward. The near surface reflection of the shortwave reaches Eastern North Dakota 29 August 18:00 UTC as the trough extends south to Oklahoma where it penetrates deeper into the ridge. Figure 7b and 7d presents a cross section and plane view of the resulting high. Due to the high pressure system the trajectory analysis indicated that smoke flowed from various fire locations in additional to stratospheric intrusion impacts to the St. Louis area (see Figure 8). Figure 9d-f depicts the vertical ozone and meteorological profiles representative of this time period (30 August). Further evidence of this trough effects on elevated ozone aloft in the sonde measurements (see Figure 2) remained until 30 August 18:00 UTC (Figure 9d-f). Thereafter a shortwave passes the area slightly to the east and cleared out the excess ozone.

Three ozone enhanced layers are present during the high pressure event as evident on 30 August (Table 3, P4 to P6). Stratospheric air descended into the middle troposphere ~500 hPa on two occasions during this time period (28 Aug and 30 Aug) from shortwaves (Figure 7d). Stratospheric impacts are indicated at ~7 to 9 km and >12 km layers with high PVU values and low RH values (Figure 9d-f, P5 and P6). NARR PVU analysis provided further proof that these are in fact stratospheric in origin. Figure 7d depicts lowering dry stratospheric air and ascending moist tropospheric air. The near surface plume (0 to 3.5 km) was traced back to southeastern agricultural fires ~5 days prior (see Figure 8), indicating a likely recirculation of air by the high pressure system. The middle-tropospheric plume P5 was determined to be from an unknown

source, potentially a recirculation of summertime ozone precursors (Cooper et al., 2006, 2007). Evidence of this layer is present in previous soundings for the week 25-29 August where all sondes show a single well-defined plume at ~5 to 9 km. The GEOS-5 and NARR potential vorticity also give no indication of what the cause for this layer is. Our hypothesis is supported by the vertical wind profiles for the week being relatively stagnant— the ozonesonde launched that day landed within 50 m of the launch site — signifying air circulation over St. Louis for the entire week increasing photochemical effects. An alternative theory is that wind shear caused the layer and it's a part of the larger plume above. The layer between the unknown plume and above (~6 to 8 km) is a layer of moist and clean air (see Figure 7d). The upper-tropospheric layer plume P6 is a combination of both a biomass burning plume and a stratospheric intrusion air mass. The lower half of the plume P6 (8 to 10 km) is dominated by stratospheric air, while the above portion of P6 (10 to 12 km) is primarily biomass burning. There is another layer of clean air above prior to reaching the tropopause. The upper-tropospheric plume P6 originated 5 days prior from high-altitude injection plumes from the California Rim Fire (25 August). The contribution of 30 August tropospheric ozone layers from Biomass burning was 10 to 80 ppbv and stratospheric air masses contributed 10 to 40 ppbv. The incorporation of high-altitude smoke injection allowed for the two mid- and upper- tropospheric polluted plumes to be characterized which contributed ~15 to 60% to layers in the total ozone column.

5 Summary and Conclusions

By incorporating balloon-borne ozonesonde observations with models, this study has quantitatively examined sources for tropospheric ozone enhancements due to Non-Controllable Ozone Sources (NCOS). In particular, the pollution impacts from stratospheric intrusions and biomass burning contributions to background tropospheric and surface ozone levels in the Midwest United States were characterized. Additionally, emphasis is placed on partitioning the contribution from western U.S. fires, central U.S. fires, and other areas to St. Louis background ozone. A chemical transport model and trajectory model were run to quantify source contribution to ozone in St. Louis, Missouri. For the region and time period of this study, 10 to 15% of the ozone enhancements stems from a stratospheric airmass contribution and 15 to 30% from biomass burning. These NCOS contributions and ozonesonde profiles can be considered as baseline ranges for the Midwest U.S. area if direct ozone measurements (sondes, airplane, ground-based) are not available. Considering U.S. fires only, 70% of the biomass burning plumes originated from the western parts of the U.S. and only 3% came from the local central U.S. emissions. Moreover, it was demonstrated that a redistribution of the biomass burning emissions injection height, with part of the emissions above the boundary layer led to a reduction of model predicted surface ozone.

In agreement with earlier studies (e.g., Fishman et al., 2014), this study has identified a generally increasing relationship between background ozone and transported pollution. We followed the definition of background ozone described in Jaffe et al. (2018) as NCOS such as lingering biomass burning and long-range transported international sources. The major contributions below 3 km were from the central U.S. fires. While 80 to 90% of the high-altitude injection smoke (above 3.5 km) originated in the western U.S. During this campaign period only 5 to 10% of the biomass burning emissions reaching St. Louis originated from the southeast and other regions.

572 This study identified that biomass burning plumes in the western U.S. can have impacts
573 on the daily atmospheric ozone column in the Midwest (10 to 80 ppbv of ozone) at a greater
574 frequency and intensity than stratospheric intrusion (10 to 25 ppbv of ozone). We show the
575 background ozone to be 55 ppbv, which was near the 30 to 50 ppbv range mentioned in Jaffe et
576 al. (2018) which is typical for the U.S. We identified a relationship between smoke plume age
577 and ozone enhancement where the high-altitude injection smoke plumes above 3.5 km generally
578 were associated with higher amounts of CO concentrations but fresher smoke regarding ozone
579 levels. In addition, we recognized that the high-altitude smoke had a higher tendency to mix with
580 stratospheric intrusions, which together doubled the ozone enhancement in the tropospheric
581 column.

582 An investigation of several individual smoke plumes has shown the importance of
583 incorporating high-altitude smoke injection in model simulations in addition to ensuring that
584 accurate biomass burning locations and temporal allocation of intensity are included in model
585 emissions. Up to 60% of the smoke plume lies above 3.5 km, and this needs to be simulated as it
586 can later be mixed down to the surface and lead to ozone exceedances days later. In addition, it
587 was shown that the incorporation of satellite-based detections of high-altitude smoke injection
588 (e.g., pyroCb activity, Peterson et al., 2014, 2017a,b) can be helpful for improve modeling results
589 and explain ozone enhancements aloft and at the surface.

590 The individual cases were selected because they are associated with common
591 meteorological situations in the Midwest leading to ozone exceedances. Evidence from the first
592 case where biomass burning is advected by a cutoff low is an example of a common flow pattern
593 that transports air masses from the west. Summertime occurrences of this synoptic situation in
594 conjunction with large wildfires in the western U.S. can lead to increases in ozone in the
595 Midwest of 10 to 80 ppbv or greater. In the second case a stratospheric air mass was shown to
596 mix with an aged wildfire plume during anticyclonic flow, a pattern that was previously found to
597 occur 40% of the time for the southcentral U.S. (Texas and the Gulf of Mexico area, Brioude et
598 al., 2007). Additionally, the test cases showed that the surface impacts were connected to
599 mechanisms causing air parcels to move downward (e.g. shortwave on 30 August). Likewise,
600 strong vertical motion was evident in bringing simulated air within the boundary to the middle
601 and upper portions of the troposphere.

602 While the results in this study highlight that Non-Controllable Ozone Sources can
603 contribute significantly to local tropospheric ozone in the Midwest, future studies must combine
604 satellite data and model integration techniques with meteorological information for a longer time
605 period, both within and outside the Midwest to better characterize NCOS contribution to U.S.
606 ozone. Good examples of how an air quality model could be used to assess NCOS has been
607 shown in Baker et al. (2016, 2018). More specifically, Baker et al. (2016, 2018) address the
608 question of regional-scale pyrogenic ozone sources. In particular, Baker et al. (2018)
609 investigated the Rim Fire, using non-sonde data, which occurred during our study period with a
610 photochemical model and their findings were similar to ours. Furthermore, as shown by
611 individual plume cases and several earlier studies (e.g. Morris et al., 2006; Brioude et al., 2007;
612 Jaffe, 2011; Lin et al., 2012; Hess and Zbinden, 2013), high-altitude smoke injection from a fire
613 can lead to long distance transport depending on weather conditions and hence impact surface
614 ozone and NAAQS attainment. Plume rise and plume injection heights are a key source of
615 uncertainty (Paugam et al., 2016), which can be reduced considerably using plume height
616 information from remote sensing tools (e.g. Peterson et al., 2017a,b; Val Martin et al., 2018).

Improved modeling techniques will be required to better characterize biomass burning transport and hence better simulate long range impacts and the possibility of unhealthy surface concentrations far from the biomass burning sources.

Acknowledgments

The authors would like to thank the SEAC^{4}RS and SEACIONS team members who gave input and guidance. A special thanks to Saint Louis University student participants in ozonesonde launches, Tim Barbeau, William Iwasko, Jackie Ringhausen, Patrick Walsh, and Jason Welsh. We also like to thank our Valparaiso University ozonesonde launch trainers Alex Kotsakis and Mark Spychala. We would also like to thank Dr. Jacky Rosati-Rowe at the U.S. EPA for editorial contributions. The data sets used in this work are publicly accessible and archived at https://tropo.gsfc.nasa.gov/seacions/ (ozonesonde data and trajectories) and https://www.nasa.gov/mission_pages/seac4rs/index.html (mission data e.g., fire emissions and flight information). This work was supported in part from NASA Grant NNX11AJ63G to Saint Louis University through its AQAST Program. D. Peterson was supported by the NASA New Investigator Program 80HQTR18T0073.

References

Baker, K. R., Woody, M. C., Tonnesen, G. S., Hutzell, W., Pye, H. O. T., Beaver, M. R., Pouliot, G., & Pierce, T. (2016). Contribution of regional-scale fire events to ozone and PM2.5 air quality estimated by photochemical modeling approaches. *Atmos. Environ.*, *140*, 539-554. doi:10.1016/j.atmosenv.2016.06.032

Baker, K. R., Woody, M. C., Valin, L., Szykman, J., Yates, E., Iraci, L., Choi, H., Soja, A., Koplitz, S., & Zhou, L. (2018). Photochemical model evaluation of 2013 California wild fire air quality impacts using surface, aircraft, and satellite data. *Sci. Total Environ., 637*, 1137–1149.

Brioude, J., Arnold, D., Stohl, A., Cassiani, M., Morton, D., Seibert, P., et al. (2013). The Lagrangian particle dispersion model FLEXPART-WRF version 3.1. *Geosci. Model Dev.*, *6*(6), 1889-1904. doi: 10.5194/gmd-6-1889-2013

Brioude, J., Cooper, O. R., Trainer, M., Ryerson, T., Holloway, J. S., Baynard, T., et al. (2007). Mixing between a stratospheric intrusion and a biomass burning plume. *Atmos. Chem. and Phys.,* (7), 4229-4235.

Colarco, P. R. (2004). Transport of smoke from Canadian forest fires to the surface near Washington, D.C.: Injection height, entrainment, and optical properties. *J. Geophys. Res.*, *109*(D6). doi: 10.1029/2003jd004248.

Cooper, O. R., Langford, A. O., Parrish, D. D., & Fahey, D. W. (2015). Challenges of a lowered US ozone standard. *Science, 348*, 1096–1097.

Cooper, O. R., Stohl, A., Trainer, M., Thompson, A. M., Witte, J. C., Oltmans, S. J., et al. (2006). Large upper tropospheric ozone enhancements above midlatitude North America during summer: In situ evidence from the IONS and MOZAIC ozone measurement network. *J. Geophys. Res.*, *111*(D24). doi: 10.1029/2006jd007306

Cooper, O. R., Trainer, M., Thompson, A. M., Oltmans, S. J., Tarasick, D. W., Witte, J. C., et al. (2007). Evidence for a recurring eastern North America upper tropospheric ozone maximum during summer. *J. Geophys. Res.*, *112*(D23). doi: 10.1029/2007jd008710

Granier, C., Bessagnet, B., Bond, T., D'Angiola, A., van der Gon, H. D., Frost, G. J., et al. (2011). Evolution of anthropogenic and biomass burning emissions of air pollutants at

global and regional scales during the 1980–2010 period. *Climatic Change*, *109*, 163-190. doi:10.1007/s10584-011-0154-1

Hess, P. G. & Zbinden, R. (2013) Stratospheric impact on tropospheric ozone variability and trends: 1990-2009. *Atmos. Chem. Phys.*, *13*, 649–674.

Hurst, D. F., Hall, E. G., Jordan, A. F., Miloshevich, L. M., Whiteman, D. N., Leblanc, T., et al. (2011). Comparisons of temperature, pressure and humidity measurements by balloon-borne radiosondes and frost point hygrometers during MOHAVE-2009. *Atmos. Meas. Tech.*, *4*, 2777–2793. doi:10.5194/amt-4-2777-2011

Davison, P. S. (2004). Estimating the direct radiative forcing due to haze from the 1997 forest fires in Indonesia. *J. Geophys. Res.*, *109*(D10). doi: 10.1029/2003jd004264

de Foy, B., Wilkins, J. L., Lu, Z., Streets, D. G., & Duncan, B. N. (2014). Model evaluation of methods for estimating surface emissions and chemical lifetimes from satellite data. *Atmos. Environ.*, *98*, 66-77. doi: 10.1016/j.atmosenv.2014.08.051

Fann, N., Alman, B., Broome, R. A., Morgan, G. G., Johnston, F. H., Pouliot, G., & Rappold, A. G. (2018). The health impacts and economic value of wildland fire episodes in the US: 2008–2012. *Sci. Total Environ., 610*, 802-809. doi: 10.1016/j.scitotenv.2017.08.024

Fann, N., Fulcher, C.M., & Baker, K. (2013). The recent and future health burden of air pollution apportioned across U.S. Sectors. *Environ. Sci. Technol.*, *47*, 3580-9. doi: 10.1021/es304831q

Ferek, R. J., Reid, J. S., Hobbs, P. V., Blake, D. R., & Liousse, C. (1998). Emission factors of hydrocarbons, halocarbons, trace gases and particles from biomass burning in Brazil. *J. Geophys. Res.*, *103*(D24), 32107. doi: 10.1029/98jd00692

Fishman, J., Belina, K. M., & Encarnación, C. H. (2014). The St. Louis Ozone Gardens: Visualizing the Impact of a Changing Atmosphere. *Bull. Amer. Meteor. Soc.*, *95*, 1171-1176.

Fromm, M., et al. (2010). The untold story of pyrocumulonimbus. *Bulletin of the American Meteorological Society*, 91, 1193-1209.

Fromm, M., D. Peterson, & Di Girolamo, L. (2019). The Primary Convective Pathway for Observed Wildfire Emissions in the Upper Troposphere and Lower Stratosphere: A Targeted Reinterpretation. *J. Geophys. Res. Atmos.*, n/a.

Holton, J. R., Haynes, P. H., McIntyre, M. E., Douglass, A. R., Rood, R. B., & Pfister, L. (1995). Stratosphere-troposphere exchange. *Rev. Geophys., 33*(4), 403. doi: 10.1029/95rg02097

Jaffe, D. (2011) Relationship between surface and free tropospheric ozone in the Western U.S. *Environ. Sci. Technol.*, *45*, 432–438.

Jaffe, D. A., Cooper, O. R., Fiore A. M., Henderson, B. H., Tonnesen, G. S., Russell, A. G., et al. (2018). Scientific assessment of background ozone over the U.S.: Implications for air quality management. *Elem. Sci. Anth.*, *6*(56). doi: https://doi.org/10.1525/elementa.309

Jaffe, D. A., & Wigder, N. L. (2012). Ozone production from wildfires: A critical review. *Atmos Environ.*, *51*, 1-10. doi: 10.1016/j.atmosenv.2011.11.063

Jaffe, D. A., Wigder, N., Downey, N., Pfister, G., Boynard, A., & Reid, S. B. (2013). Impact of wildfires on ozone exceptional events in the western US. *Environ. Sci. Technol.*, *47*, 11065–11072.

Kley, D., Crutzen, P. J., Smit, H. G. J., Vömel, H., Oltmans, S. J., Grassl, H., & Ramanathan, V. (1996). Observations of near-zero ozone concentrations over the convective Pacific: Effects on air chemistry. *Science*, *274*, 230–233. https://doi.org/10.1126/science.274.5285.230.

Komhyr, W. D., Barnes, R. A., Brothers, G. B., Lathrop, J. A., & Opperman, D. P. (1995). Electrochemical concentration cell ozonesonde performance evaluation during STOIC 1989. *J. Geophys. Res., 100*(D5), 9321-9244.

Komhyr, W. D., Oltmans, S., & Grass, R. D. (1986). Atmospheric Ozone at South Pole, Antarctica, in 1986. *J. Geophys. Res., 93*(D5), 5167-5184. Doi:10.1029/JD093iD05p05167

Kuang, S., Newchurch, M. J., Burris, J., Wang, L., Knupp, K., & Huang, G. (2012). Stratosphere-to-troposphere transport revealed by ground-based lidar and ozonesonde at a midlatitude site. *J. Geophys. Res.-Atmos.*, *117*(D18), n/a-n/a. doi: 10.1029/2012jd017695

Lahoz, W. A., Errera, Q., Swinbank, R., & Fonteyn, D. (2007), Data assimilation of stratospheric constituents: A review, *Atmos. Chem. Phys.*, *7*, 5745–5773. doi:10.5194/acp-7-5745-2007.

Lal, S., Venkataramani, S., Chandra, N., Cooper, O.R., Brioude, J., & Naja, M. (2014) Transport effects on the vertical distribution of tropospheric ozone over western India. *J. Geophys. Res. Atmos., 119*(16), 10012–10026. DOI: https://doi. org/10.1002/2014jd021854

Langford, A. O., Aikin, K. C., Eubank, C. S. & Williams, E. J. (2009). Stratospheric contribution to high surface ozone in Colorado during springtime. *Geophys. Res. Lett.*, *36*, L12801.

Langford, A. O., Alvarez, R. J., Brioude, J., Evan, S., Iraci, L. T., Kirgis, G., et al. (2018). Coordinated profiling of stratospheric intrusions and transported pollution by the Tropospheric Ozone Lidar Network (TOLNet) and NASA Alpha Jet experiment (AJAX): Observations and comparison to HYSPLIT, RAQMS, and FLEXPART. *Atmos. Environ.*, *174*, 1–14. DOI: https://doi.org/10.1016/j. atmosenv.2017.11.031

Langford, A. O., Senff, C. J., Alvarez, R. J., Brioude, J., Cooper, O. R., Holloway, J. S., et al. (2015). An overview of the 2013 Las Vegas Ozone Study (LVOS): Impact of stratospheric intrusions and long-range transport on surface air quality. *Atmos. Environ., 109*, 305–322. DOI: https:// doi.org/10.1016/j.atmosenv.2014.08.040

Larkin, N. K., Raffuse, S. M., & Strand, T. M. (2014). Wildland fire emissions, carbon, and climate: US emissions inventories. *For. Ecol. Manag.*, 317, 61–69. doi:10.1016/J.FORECO.2013.09.012

Li, K., Jacob, D.J., Liao, H., Shen, L., Zhang, Q., & Bates, K.H. (2019). Anthropogenic drivers of 2013-2017 trends in summer surface ozone in China. *Proceedings of the National Academy of Sciences*, *116*(2), 422–427. https://doi.org/10.1073/pnas.1812168116

Lin, M., Fiore, A. M., Horowitz, L. W., Langford, A. O., Oltmans, S. J., Tarasick, D., & Rieder, H. E. (2015) Climate variability modulates western US ozone air quality in spring via deep stratospheric intrusions. *Nature Comm.*, *6*, 7105, doi:10.1038/ncomms8105.

Liousse, C., Penner, J. E., Chuang, C., Walton, J. J., Eddleman, H., & Cachier, H. (1996). A global three-dimensional model study of carbonaceous aerosols. *J. Geophys. Res., 101*(D14), 19411. doi: 10.1029/95jd03426

Liu, J. C., Pereira, G., Uhl, S. A., Bravo, M. A. & Bell, M. L. (2015). A systematic review of the physical health impacts from non-occupational exposure to wildfire smoke. *Environ. Res.*, *136*, 120–132. https://doi.org/10.1016/j.envres.2014.10.015

Liu, J. C., Mickley, L. J., Sulprizio, M. P., Yue, X., Peng, R. D., Dominici, F. & Bell M. L. (2016). Future respiratory hospital admissions from wildfire smoke under climate change in the Western US. *Environ. Res. Lett.*, *11*(10.1088), 1748-9326.

Liu, J. C., Wilson, A., Mickley, L. J., Dominici, F., Ebisu, K., Wang, Y., et al. (2017). Wildfire-specific Fine Particulate Matter and Risk of Hospital Admissions in Urban and Rural

753 Counties. *Epidemiology*, *28*(1), 77–85. https://doi.org/10.1097/EDE.0000000000000556
754 Liu, XX, Zhang, Y, Huey, L. G., Yokelson, R. J., Wang, Y., Jimenez, J.L., et al. (2016).
755 Agricultural fires in the southeastern US during SEAC4RS: Emissions of trace gases and
756 particles and evolution of ozone, reactive nitrogen, and organic aerosol. *J. Geophys. Res.*
757 *Atmos.*, *121*(12): 7383– 7414. DOI: https://doi.org/10.1002/2016jd025040
758 McCarty, J.L., Justice, C.O., & Korontzi, S. (2007). Agricultural burning in the Southeastern
759 United States detected by MODIS. *Remote Sens. Environ.*, 108(2), 151– 162. DOI:
760 https://doi.org/10.1016/j.rse.2006.03.020
761 McClure, C. D. & Jaffe, D. A. (2018). US particulate matter air quality improves except in
762 wildfire-prone areas. *Proceedings of the National Academy of Sciences*, 115(31), 7901–
763 7906. https://doi.org/10.1073/pnas.1804353115
764 Mesinger, F., DiMego, G., Kalnay, E., Mitchell, K., Shafran, P. C., Ebisuzaki, W., et al. (2006).
765 North American Regional Reanalysis. *Bull. Am. Meteorol. Soc.*, 87(3), 343-360. doi:
766 10.1175/bams-87-3-343
767 Moeini, O., Tarasick, D. W., McElroy, C. T., Liu, J., Osman, M., Thompson, A. M., Parrington,
768 M., Palmer, P. I., Johnson, B. J., Oltmans, S. J., Merrill, J. (2020). Estimating wildfire-
769 generated ozone over North America using ozonesonde profiles and a differential back
770 trajectory technique, *Atmos. Environ.: X*, 7, 100078,
771 https://doi.org/10.1016/j.aeaoa.2020.100078.
772 Morris, G. A., Hersey, S., Thompson, A. M., Pawson, S., Nielsen, J. E., Colarco, P. R., et al.
773 (2006). Alaskan and Canadian forest fires exacerbate ozone pollution over Houston,
774 Texas, on 19 and 20 July 2004. *J. Geophys. Res.*, *111*(D24). doi: 10.1029/2006jd007090
775 Ott, L. E., Duncan, B. N., Thompson, A. M., Diskin, G., Fasnacht, Z., Langford, A. O., et al.
776 (2016). Frequency and impact of summertime stratospheric intrusions over Maryland
777 during DISCOVER-AQ (2011): New evidence from NASA's GEOS-5 simulations. *J.*
778 *Geophys. Res. Atmos., 121*(7), 3687–3706. DOI: https://doi. org/10.1002/2015jd024052
779 Parrish, D. D., Aikin, K. C., Oltmans, S. J., Johnson, B. J., Ives, M., & Sweeny, C. (2010).
780 Impact of transported background ozone inflow on summertime air quality in a California
781 ozone exceedance area. *Atmos. Chem. Phys*., *10*(20), 10093–10109. DOI: https://doi. org/
782 10.5194/acp-10-10093-2010
783 Parrish, D. D., Lamarque, J. F., Naik, V., Horowitz, L., Shindell, D. T., Staehelin, J., et al.
784 (2014). Long-term changes in lower tropospheric baseline ozone concentrations:
785 Comparing chemistry-climate models and observations at northern midlatitudes. *J.*
786 *Geophys. Res. Atmos., 119*(9), 5719– 5736. DOI: https://doi.org/10.1002/2013jd021435
787 Parrish, D. D., Law, K. S., Staehelin, J., Derwent, R., Cooper, O. R., Tanimoto, et al. (2012).
788 Long-term changes in lower tropospheric baseline ozone concentrations at northern mid-
789 latitudes. *Atmos. Chem. Phys., 12*, 11485–11504. DOI: https://doi.org/10.5194/acp-12-
790 11485-2012
791 Paugam R., Wooster M., Freitas S., & Val Martin M. (2016) A review of approaches to estimate
792 wildfire plume injection height within large-scale atmospheric chemical transport models.
793 *Atmos. Chem. Phys.*, *16*, 907-925. doi: 10.5194/acp-16-907-2016
794 Peterson, D. A., Campbell, J. R., Hyer, E., Fromm, M., Kablick, G., Cossuth, J., & DeLand, M.
795 (2018). Wildfire-driven thunderstorms cause a volcano-like stratospheric injection of
796 smoke. *NPJ Clim. Atmos. Sci.*, *1*(30). doi:10.1038/s41612-018-0039-3
797 Peterson, D. A., Hyer, E. J., Campbell, J. R., Fromm, M. D., Hair, J. W., Butler, C. F., & Fenn,
798 M. A. (2015). The 2013 Rim Fire: Implications for Predicting Extreme Fire Spread,

Pyroconvection, and Smoke Emissions. *Bull. Am. Meteorol. Soc.*, *96, 229-247*. doi: 10.1175/bams-d-14-00060.1

Peterson, D. A., M. D. Fromm, J. E. Solbrig, E. J. Hyer, M. L. Surratt, & Campbell, J. R. (2017a). Detection and Inventory of Intense Pyroconvection in Western North America using GOES-15 Daytime Infrared Data. *J. Appl. Meteorol. Climatol.*, 56, 471-493.

Peterson, D. A., Hyer E. J., Campbell, J. R., Solbrig, J. E., & Fromm, M. D. (2017b) A conceptual model for development of intense pyrocumulonimbus in western north america. *Mon. Weather Rev.*, 145, 2235-2255. doi: 10.1175/mwr-d-16-0232.1

Peterson, D., Hyer, E., & Wang, J. (2014). Quantifying the potential for high-altitude smoke injection in the North American boreal forest using the standard MODIS fire products and subpixel-based methods. *J. Geophys. Res.-Atmos*, *119*, 2013JD021067.

Rappold, A. G., Reyes, J., Pouliot, G., Cascio, W. E., & Diaz-Sanchez, D. (2017) Community vulnerability to health impacts of wildland fire smoke exposure. *Environ. Sci. Technol.*, *51*, 6674-6682. doi: 10.1021/acs.est.6b06200

Reid, C. E., Brauer, M., Johnston, F. H., Jerrett, M., Balmes, J. R., & Elliott, C. T. (2016). Critical review of health impacts of wildfire smoke exposure. *Environ. Health Perspect.*, *124*, 1334.

Reid, J. S., Hyer, E., Prins, E. M., Westphal, D. L., Zhang, J., Wang, J., et al. (2009). Global Monitoring and Forecasting of Biomass-Burning Smoke: Description of and Lessons from the Fire Locating and Modeling of Burning Emissions (FLAMBE) Program. *IEEE J. Sel. Top. Appl.*, *2*(3), 144–162. Doi:10.1109/JSTARS.2009.2027443.

Rienecker, M. M., Suarez, M. J., Todling, R., Bacmeister, J., Takacs, L., Liu, H.-C., et al. (2008). The GEOS-5 Data Assimilation System—Documentation of Versions 5.0.1, 5.1.0, and 5.2.0. Technical Report Series on Global Modeling and Data Assimilation, 27.

Silva, R. A., West, J. J., Zhang, Y., Anenberg, S. C., Lamarque, J.-F., Shindell, D. T., et al. (2013). Global premature mortality due to anthropogenic outdoor air pollution and the contribution of past climate change. *Environ. Res. Lett., 8*(3). DOI: https://doi. org/10.1088/1748-9326/8/3/034005

Simon, H., Reff, A., Wells, B., Xing, J., & Frank, N. (2015). Ozone trends across the United States over a period of decreasing NOx and VOC emissions. *Environ. Sci. Technol.*, *49*(1), 186–195. DOI: https://doi. org/10.1021/es504514z

Skamarock, W. C., Klemp, J. B., Dudhia, J., Gill, D. O., Barker, D. M., Duda, M. G., et al. (2008). A description of the Advanced Research WRF Version 3. Technical Note NCAR/ TN-475+STR, National Center for Atmospheric Research, Boulder, Colorado, 113 pp.

Stajner, I., Wargan, K., Pawson, S., Hayashi, H., Chang, L.-P., Hudman, R. C., et al. (2008). Assimilated ozone from EOS-Aura: Evaluation of the tropopause region and tropospheric columns. *J. Geophys. Res.*, *113*(D16). doi: 10.1029/2007jd008863

Stauffer, R. M., Morris, G. A., Thompson, A. M., Joseph, E., Coetzee, G. J. R., & Nalli, N. R. (2014). Propagation of radiosonde pressure sensor errors to ozonesonde measurements. *Atmos. Meas. Tech.*, *7*, 65–79. doi:10.5194/amt-7-65-2014.

Stocks, B. J., Fosberg, M. A., Lynham, T. J., Mearns, L., Wotton, B. M., Yan, F., et al. (1998) Climate change and forest fire potential in russian and canadian boreal forest. *Climate Change*, *38*, 1-13.

Stohl, A. (2003). A backward modeling study of intercontinental pollution transport using aircraft measurements. *J. Geophys. Res.*, *108*(D12). doi: 10.1029/2002jd002862

Strode, S. A., Rodriguez, J. M., Logan, J. A., Cooper, O. R., Witte, J. C., Lamsal, L. N., et al.

(2015). Trends and variability in surface ozone over the United States. *J. Geophys. Res.-Atmos.*, *120*(17), 9020–9042. DOI: https://doi.org/10.1002/2014JD022784

Sullivan, J. T., McGee, T. J., Thompson, A. M., Pierce, R. B., Sumnicht, G. K., Twigg, L., Eloranta, E., & Hoff, R. M. (2015). Characterizing the lifetime and occurrence of stratospheric-tropospheric exchange events in the rocky mountain region using high-resolution ozone measurements. *J. Geophys. Res.-Atmos., 120*(24), 12410–12424. DOI: https://doi. org/10.1002/2015jd023877

Thompson, A. M., Allen, A. L., Lee, S., Miller, S. K., & Witte, J. C. (2011a). Gravity and Rossby wave signatures in the tropical troposphere and lower stratosphere based on Southern Hemisphere Additional Ozonesondes (SHADOZ), 1998–2007. *J. Geophys. Res.*, *116*(D5). doi: 10.1029/2009jd013429

Thompson, A. M., Oltmans, S. J., Tarasick, D. W., von der Gathen, P., Smit, H. G. J., & Witte, J. C. (2011b). Strategic ozone sounding networks: Review of design and accomplishments. *Atmos. Environ.*, *45*(13), 2145-2163. doi: 10.1016/j.atmosenv.2010.05.002

Thompson, A. M., Smit, H. G., Witte, J. C., Stauffer, R. M., Johnson, B. J., Morris, G., et al. (2019). Ozonesonde Quality Assurance: The JOSIESHADOZ (2017) Experience. *Bull. Amer. Meteor. Soc.*, *100*, 155–171. https://doi.org/10.1175/BAMS-D-17-0311.1.

Thompson, A. M., Stone, J. B., Witte, J. C., Miller, S. K., Oltmans, S. J., Kucsera, T. L., et al. (2007). Intercontinental Chemical Transport Experiment Ozonesonde Network Study (IONS) 2004: 2. Tropospheric ozone budgets and variability over northeastern North America. Journal of Geophysical Research, 112(D12). doi: 10.1029/2006jd007670

Toon, O. B., Maring, H., Dibb, J., Ferrare, R., Jacob, D. J., Jensen, E. J., et al. (2016). Planning, implementation, and scientific goals of the studies of emissions and atmospheric composition, clouds and climate coupling by regional surveys (SEAC4RS) field mission. *J. Geophys. Res.-Atmos.*, *121*, 4967–5009.

Travis, K. R., Jacob, D. J., Fisher, J. A., Kim, P. S., Marais, E. A., Zhu, L., et al. (2016). Why do models overestimate surface ozone in the Southeast United States? *Atmos. Chem. Phys.*, *16*, 13561–13577, https://doi.org/10.5194/acp-16-13561-2016.

U.S. Environmental Protection Agency (US EPA). (2013). Integrated Science Assessment (ISA) of Ozone and Related Photochemical Oxidants (Final Report, Feb 2013). Washington, DC: U.S. Environmental Protection Agency. EPA/600/R-10/076F. Available at: https://cfpub.epa.gov/ncea/isa/recordisplay. cfm?deid=247492 Accessed October 27, 2019.

U.S. Environmental Protection Agency (US EPA). (2015). Implementation of the 2015 Primary Ozone NAAQS: Issues Associated with Background Ozone, White Paper for Discussion. Washington, DC: U.S. Environmental Protection Agency. Available at: https://www.epa.gov/sites/production/ files/2016–03/documents/whitepaper-bgo3-final. pdf Accessed October 27, 2019.

Val Martin, M., Kahn, R. A., Logan, J. A., Paugam, R., Wooster, M., & Ichoku, C. (2012). Space-based observational constraints for 1-D fire smoke plume-rise models. *J. Geophys. Res.-Atmos.*, *117*(D22), n/a-n/a. doi: 10.1029/2012jd018370

Val Martin M., Kahn R. A., & Tosca M. G. (2018) A Global Analysis of Wildfire Smoke Injection Heights Derived from Space-Based Multi-Angle Imaging. *Remote Sens.*, *10*, 1609. doi:10.3390/rs10101609.

Wagner, N. L., Brock, C. A., Angevine, W. M., Beyersdorf, A., Campuzano-Jost, P., Day, D., et al. (2015). In situ vertical profiles of aerosol extinction, mass, and composition over the

891 southeast United States during SENEX and SEAC4RS: observations of a modest aerosol
892 enhancement aloft. *Atmos. Chem. Phys.*, *15*, 7085–7102. https://doi.org/10.5194/acp-15-
893 7085-2015.
894 Wargan, K., Pawson, S., Olsen, M. A., Witte, J. C., Douglass, A. R., Ziemke, J. R., et al. (2015).
895 The global structure of upper troposphere-lower stratosphere ozone in GEOS-5: A
896 multiyear assimilation of EOS Aura data. *J. Geophys. Res.-Atmos.*, *120*, 2013-2036. doi:
897 10.1002/2014jd022493
898 Waugh, D. W., & Funatsu, B. M. (2003). Intrusions into the Tropical Upper Troposphere: Three-
899 Dimensional Structure and Accompanying Ozone and OLR Distributions. *J. Atmos. Sci.*,
900 60, 637-653.
901 Westerling, A. L., Hidalgo, H. G., Cayan, D. R. & Swetnam, T. W. (2006). Warming and earlier
902 spring increase western US forest wildfire activity. *Science*, *313*(5789), 940–943.
903 Westerling, A. L. (2016) Increasing western US forest wildfire activity: Sensitivity to changes in
904 the timing of spring. *Philos. Trans. R. Soc. B. Biol. Sci., 371*(1696):20150178.
905 Wilkins, J. L., Pouliot, G., Foley, K., Appel, W., & Pierce, T. (2018). The impact of US wildland
906 fires on ozone and particulate matter: a comparison of measurements and CMAQ model
907 predictions from 2008 to 2012. *Int. J. Wildland Fire*, *27*, 684–698.
908 https://doi.org/10.1071/WF18053, 2018.
909 Zhu, L., Jacob, D. J., Kim, P. S., Fisher, J. A., Yu, K., Travis, K. R., et al. (2016) Observing
910 atmospheric formaldehyde (HCHO) from space: validation and intercomparison of six
911 retrievals from four satellites (OMI, GOME2A, GOME2B, OMPS) with SEAC4RS
912 aircraft observations over the southeast US. *Atmos. Chem. Phys.*, *16*, 13477–13490.
913 https://doi.org/10.5194/acp-16-13477-2016, 2016.
914

Figure 1. Study area map with FLEXPART-WRF model domain. Rectangles mark the WRF domains D1 which has a horizontal resolution of 12 km and D2 (4 km resolution). SEACIONS locations are marked by black circles (St. Louis, Missouri station (STL) is a gray circle). Wildfire emissions from FLAMBE, August-September 2013, with eleven Pyro convective and five high-altitude injection elevated smoke plume activity areas are marked, red crosses indicate pyroCb plumes which transport smoke into the upper troposphere and lower stratosphere. Blue crosses indicate high-altitude injection of smoke in the absence of large pyroCb which transport smoke into the mid-troposphere).

Figure 2. Ozonesondes in support of SEACIONS were launched at the Saint Louis University ozonesonde station located at the James S. McDonnell Planetarium in Forest Park (90.27˚W, 38.63˚N, 181 m asl), 5 km west of downtown St. Louis. Vertical tropospheric profiles at ~18:30 UTC (1:30 p.m. Local time) ozone profiles are averaged vertically every 500 m and shown below the thermal tropopause level (~15 km). Cases of ozone enhancements above the background (~55 ppbv) are shown by source origin: the gray box for Stratospheric-Tropospheric Transport (STT), the solid black line boxes for biomass burning (BB), and the dashed line black boxes for combined STT and BB.

Figure 3. Biomass burning emissions of carbon monoxide (CO) estimated by FLAMBE in units of Gg per km^2 per hour in North America during SEACIONS, 8 Aug to 22 Sept 2013. FLAMBE emissions are displayed on the model grid which has a resolution of 0.25˚ per cell. Only cells with emissions above 2,000 kg are shown.

Figure 4. A time series of FLAMBE emissions (mass/time) converted to particles released in FLEXPART-WRF (# of particles or particle count). Each 500 kg of mass is converted to 1 particle in FLEXPART-WRF simulations. Locations emitting less than 500 kg only emit a single particle. Arrows represent the duration of two of the largest wildfires (Rim Fire and Beaver Creek) with relevance to SEACIONS with other fires (Emigrant Fire and Pony/Elk Complex) contributing to those time frame emissions indicated. The dotted line is the California Rim Fire (37.85˚N, 120.083˚W) 17-31 August 2013, and the solid line is the Idaho Beaver Creek (43.593˚N, 114.684˚W) 7-21 August 2013. Note: Beaver Creek and Pony/Elk Complex occurred nearly at the same time and were fewer than 100 km apart in distance. While, the Emigrant Fire contributed a significant amount of emissions during its occurrence at the same time as the Rim Fire but was much smaller in magnitude.

Figure 5. FLEXPART-WRF Biomass burning (BB) CO concentrations and age are simulated, binning trajectories over St. Louis within a 2.5˚ x 2.5˚ grid box and averaged vertically 500 m with daily temporal resolution. FLAMBE emissions of BB CO are converted into particle amounts and are released. (a) The base simulation, Boundary Layer Simulation, releases emissions within the PBL, (b) NRL's adjusted pyro-convention scheme is implemented, PyroCb Simulation, particles are released from pyroCbs and high-altitude injection as specified in Table 1, and (c). The combined (a) and (b). With panels (d-f), corresponding to plume ages in simulations. The average BB CO g cm^{-3} per grid cell (top) lighter shading indicated higher concentration and transported CO plume ages (bottom) lighter shading indicates older air.

Figure 6. Series of daily synoptic atmospheric plane slices at 500 hPa at 7:00 UTC for preceding conditions to individual transport cases (a-c) 21 August 2013 (d-f) 30 August 2013.

957 **Figure 7.** Atmospheric plane slices from NARR at 500 hPa at 18:00 UTC (a) 21 August 2013 (b)
958 30 August 2013. Vertical Cross sections at 90˚ W, 20-60˚ N 18:00 UT (c) 21 August 2013 (d) 30
959 August 2013. Blue contour lines show Potential Vorticity (PV) 10^6 PVU, Relative Humidity
960 (RH) below 30% is shaded from light to dark, with darker shades representing the dryer air. The
961 black lines on (a) and (b) are pressure height contours in m. While, the black lines on (c) and (d)
962 represent potential temperature (isentropic surfaces) in K. Biomass burning sources tend to have
963 low PV and can have moderate RH levels for pyroCbs, while stratospheric air masses have high
964 PV and low RH. The blue dashed line PV contour (1.5 PV) shows the approximate boundary
965 between stratospheric and tropospheric air masses. Arrows (green) show air-mass transport
966 patterns from Stratospheric-Tropospheric Transport (STT) and from Biomass Burning (BB).

968 **Figure 8.** NOAA Hazard Management System (HMS) and Smoke Product analysis of smoke (a)
969 21 Aug 2013 and (b) 30 Aug 2013. Below, three-day backward FLEXPART-WRF trajectories
970 corresponding to each episode is provided (c) 21 Aug 2013 and (d) 30 Aug 2013. Additional
971 trajectories are placed in the data archive at https://tropo.gsfc.nasa.gov/seacions/.

972 **Figure 9.** Vertical tropospheric profiles over St. Louis at ~18:30 to 19:30 UTC for selected test
973 cases 21 August 2013 and 30 August 2013. Labels P1 to P6 correspond to plume information in
974 Table 3. Ozone measured from the ozonesonde in ppb are shown as a black line. Panel (a) and
975 (d), the green line RH %. Panel (b) and (e), the blue line represents the GEOS-5 modeled
976 Potential Vorticity 10^6 PVU. Panel (c) and (f), the FLEXPART-WRF modeled CO biomass
977 burning g cm^{-3}, for each simulation the PYRO simulation is red, and BASELINE simulation in
978 gray. Refer to Figure 2 for corresponding ozonesonde curtain plots.
979

980 **Table 1.** Elevated smoke plumes escaping the planetary boundary layer identified by the Naval
981 Research laboratory satellite detection algorithm for high-altitude injection during the Studies of
982 Emissions and Atmospheric Composition, Clouds and Climate Coupling by Regional Surveys
983 (SEAC4RS) in the summer 2013. Smoke plumes detected are categorized: 1. A pyroconvective
984 plume containing smoke reaching the stratosphere (~10 to 15 km) or 2. A high-altitude plume
985 containing smoke reaching into the middle troposphere (~5 to 9 km).

986

Date	Time (UTC)	Lat	Lon	State	Fire name	Plume type
7 Aug 2013	22:15	42.71	-123.66	OR	Big Windy Complex	High-altitude
8 Aug 2013	n/A	43.46	-114.55	ID	Beaver Creek	Pyroconvective
8 Aug 2013	n/A	43.42	-114.85	ID	McCan	Pyroconvective
9 Aug 2013	22:41	43.29	-115.55	ID	Pony/Elk	Pyroconvective
10 Aug 2013	21:00	43.36	-115.45	ID	Pony/Elk	Pyroconvective
12 Aug 2013	21:00	43.29	-115.55	ID	Pony/Elk	Pyroconvective
12 Aug 2013	23:00	43.62	-114.51	ID	Beaver Creek	Pyroconvective
13 Aug 2013	23:41	43.50	-115.43	ID	Pony/Elk	Pyroconvective
16 Aug 2013	21:41	45.66	-114.78	ID	Gold Pan Complex	Pyroconvective
16 Aug 2013	23:41	43.62	-114.51	ID	Pony/Elk	High-altitude
16 Aug 2013	23:41	43.46	-114.55	ID	Beaver Creek	Pyroconvective
19 Aug 2013	22:50	45.20	-110.69	MT	Emigrant	High-altitude
19 Aug 2013	23:15	37.86	-120.09	CA	Rim	Pyroconvective
21 Aug 2013	22:41	37.86	-120.09	CA	Rim	Pyroconvective
22 Aug 2013	21:30	41.04	-123.47	CA	Corral Complex	High-altitude
25 Aug 2013	17:00	37.91	-120.00	CA	Rim	High-altitude

987 **Table 2.** Simulated stratospheric air masses entering the troposphere (stratospheric intrusion)
988 over St. Louis, Missouri during August and September 2013.

Date	Time (UTC)	Duration (hr)	Height (hPa)	Extent	Meteorology
3 Aug 2013	03:30	21	580	Shallow	Frontal passage
7 Aug 2013	13:30	28	690	Deep	Shortwave
10 Aug 2013	02:30	34	800	Deep	Shortwave
12 Aug 2013	18:30	28	500 to 850	Deep	Frontal passage
14 Aug 2013	06:30	180	600	Shallow	Cutoff low
23 Aug 2013	16:30	9	500	Shallow	Shortwave
28 Aug 2013	21:30	18	480	Shallow	Shortwave
30 Aug 2013	08:30	94	500	Shallow	Shortwave
3 Sept 2013	12:30	30	700 to 1000	Deep	Frontal passage
6 Sept 2013	09:30	41	600	Shallow	Shortwave
12 Sept 2013	16:30	10	800	Deep	Frontal passage
15 Sept 2013	20:30	48	800 to 1000	Deep	Frontal passage
22 Sept 2013	00:30	94	900	Deep	Frontal passage

989 **Table 3.** Ozone (O_3) enriched plumes identified over St. Louis, Missouri using ozonesondes
990 vertical profile measurements for two episodes. Included are the simulated biomass burning
991 plumes and stratospheric air masses entering the troposphere (stratospheric intrusion (SI))
992 concentrations of a carbon monoxide (CO) tracer for each plume. Plume ID corresponds to
993 labeling in Figure 9.

994

Plume ID	Date	Source	Plume height	Smoke age	BASELINE simulation	PYRO Simulation	Sonde RH	Sonde O_3	Excess O_3
			AGL km	days	CO ppm	CO ppm	%	ppb	ppb
P1	21 Aug	ID Beaver Creek	2 to 5.5	5.8	2.4	14	10	65	10
P2	21 Aug	MT Emigrant	7 to 9	2.6	0	5.2	5	85	25
P3	21 Aug	pyroCb and SI	11	1.2	0	0.63	20	65	10
P4	30 Aug	SE US Ag. Fire	0 to 2.5	5.1	6.6	0.83	85	65	10
P5	30 Aug	Unidentified	5 to 7	6.7	0	0.35	10	100	45
P6	30 Aug	CA Rim Fire and SI	8 to 12	5.3	0	6.8	15	140	80

995